Differences in excitatory and inhibitory neuron oxygen metabolism elucidated by intrinsic optical imaging and optogenetics in awake mice

by

Andrew E. Toader

Submitted to the Graduate Faculty of the

University Honors College in partial fulfillment

of the requirements for the degree of

Bachelor of Science in Engineering

University of Pittsburgh

2022

UNIVERSITY OF PITTSBURGH

SWANSON SCHOOL OF ENGINEERING

This thesis was presented

by

Andrew E. Toader

It was defended on

April 13, 2022

and approved by

Dr. Murat Ackakaya, Associate Professor, Electrical and Computer Engineering

Dr. Liang Zhan, Assistant Professor, Electrical and Computer Engineering

Dr. Mitsuhiro (Hiro) Fukuda, Assistant Professor, Radiology

Dr. Jana Kainerstorfer, Associate Professor, Biomedical Engineering, Carnegie Mellon University

Thesis Advisor: Dr. Alberto Vazquez, Associate Professor, Radiology and Bioengineering

Difference in excitatory and inhibitory neuron oxygen metabolism elucidated by intrinsic optical imaging and optogenetics in awake and anesthetized mice

Andrew E. Toader

University of Pittsburgh, 2022

Neurons rely on a continuous supply of oxygen to sustain their function. Many studies have shown that metabolic consumption is proportional to overall brain activity, but it is not clear whether oxygen metabolism is different between excitatory and inhibitory neurons, the two major neuronal subtypes. It is thought that dysfunction in excitatory and inhibitory neurons plays a key role in the pathologies of various diseases including Epilepsy and Alzheimer's Disease. This work examined potential differences in the cerebral rate of oxygen metabolism ($CMRO_2$) between excitatory and inhibitory cortical neurons using optical imaging methods sensitive to blood oxygenation. Manipulation of excitatory and inhibitory neurons was facilitated using optogenetics to selectively manipulate the activity of these neurons. Our results suggest that optogenetic activation of excitatory neurons is less metabolically expensive than optogenetically activating inhibitory neurons by as much as a factor of 6.9 (range from 0.76 to 6.9). The low-end of this range does not consider that excitatory neurons outnumber inhibitory neurons in cortex by about 4:1, still providing support for inhibitory neurons consuming more oxygen than excitatory neurons under awake conditions. We compared these results to our previous study conducted under light ketamine anesthesia using similar experimental procedures where optogenetic activation of inhibitory neurons was more metabolically expensive than activating excitatory neurons by a factor of 2.6. Understanding the oxygen consumption of neuronal subtypes can elucidate

functional disturbances in areas across the brain and may aid in the discovery of various therapeutic modalities for diseases that preferentially target genetically distinct populations of neurons.

Table of Contents

List of Tables

List of Figures

Preface

I would like to thank Dr. Alberto Vazquez for his support and mentorship throughout my undergraduate studies. I would also like to Drs. Hiro Fukuda and Jana Kainerstorfer for their input and support during the development and experimental portions of the project. Their expertise in the sensitivity of optical systems to changes in hemoglobin oxygenation has been invaluable. I would also like to thank Dr. Murat Ackakaya for his input on possible uses of machine learning for analysis, Dr. Liang Zhan for his suggestions on determining sample sizes and choosing control groups, and Dr. Ervin Sejdic for this suggestions on my experimental setup and general comments on my undergraduate research work. Additionally, I would like to thank Drs. Mioara Manole and Joan Mavrniac for the time they spent reviewing this work. Funding for this project was provided by the National Institutes of Health (NIH) NIH-R01-NS094404.

1.0 Introduction

My goal in this work is to examine differences in oxygen metabolism across different neuronal populations. Neurons rely on oxygen to sustain their function, thus the continuous supply of oxygen and glucose by blood is necessary to this end. I use optogenetics to selectively activate distinct neuronal populations in live mice. Determining oxygen metabolism requires multiple measurements to be combined, using a model based on conservation of mass. In this chapter, I introduce general concepts underlying this work. In chapter 2, I introduce the model and simulation results to showcase how the model works. In chapter 3, I describe the methods used, including animal models, animal surgery, data acquisitions methods, data analysis methods and experimental design. Our experimental design has three parts. First, I tested the model using data with a known physiological perturbation to ensure that the imaging equipment can be sensitive to changes in oxygen metabolism. Then, I conducted experiments in mice that target two large and distinct populations of neurons. Last, I conducted experiments in mice that target sub-populations of neurons. Chapter 4 presents my results in the aforementioned order, and in Chapter 5, I discuss the findings obtained and future directions.

1.1 Neurons and Oxygen Metabolism

Neurons are the principal cellular units of the brain, however they lack energy stores to sustain their function. As a result, the brain relies on the continuous supply of oxygen and glucose provided by the vasculature. Oxygen is metabolized in the mitochondria of cells and acts as the

final electron carrier in the Electron Transport Chain (ETC). In normoxic environments, cellular respiration can produce up to 38 Adenosine Triphosphate (ATP) molecules, the energy substrate of cells, which neurons subsequently use for signaling processes such as action potential propagation. In hypoxic environments, the ETC as well as the Citric Acid Cycle are downregulated, as oxygen is not able to accept the electrons in the final step of the ETC. Thus, the number of ATP produced decreases to as little as 4 ATP per glucose molecule in hypoxic environments. This drastic decrease in ATP production in hypoxic environments makes it evident why oxygen metabolism is vital to neuronal health and firing.

Two major types of neurons exist in the mammalian brain: excitatory neurons, which promote firing of connected neurons, and inhibitory neurons, which suppress the firing of other neurons. Excitatory neurons make up about 80-85% of all neurons in cortex and rely on the neurotransmitter glutamate to activate down-stream neurons. Excitatory neurons tend to be large with extensive dendritic and axonal arbors that span local and distal networks, often in opposite hemispheres or sub-cortical regions. Inhibitory neurons are much less numerous, comprising 15-20% of all cortical neurons. Their axonal and dendritic arbors tend to remain local, and they rely on the neurotransmitter GABA to inhibit the activity of down-stream connected neurons (1).

Many studies have shown that metabolic consumption is proportional to overall brain activity (2-4), but it is not known whether oxygen metabolism is different in excitatory and inhibitory neurons, especially under awake conditions. Understanding the metabolic consumption of neurons can lead to a greater insight into neuronal physiology and brain homeostasis, such as whether the vasculature is preferentially responsive to the metabolic demands of specific neuronal sub-types.

The cerebral metabolic rate of oxygen ($CMRO_2$) is the metric used to quantify the oxygen consumption in a region of interest. Oxygen is metabolized in mitochondria and traditional methods to measure oxygen consumption rely on direct measurements of tissue oxygen using positron emission tomography (PET) or polarographic oxygen microelectrodes (5, 6). Oxygen is delivered to tissue by blood at the capillary level, such that the rate of oxygen consumption depends on cerebral blood flow (CBF). Because there is no net storage or accumulation of oxygen in tissue, the amount of oxygen in blood is generally in equilibrium with tissue oxygen.

1.2 Imaging Oxygen Metabolism

Hemoglobin, the carrier of oxygen in blood, is a strong absorber of visible light, and its absorption properties depend on the incident light wavelength as well as the number of oxygen molecules bound to it (i.e., oxygen saturation) (7). Hence, optical imaging methods can be used to measure the oxygenation state of hemoglobin and therefore the oxygenation level of blood as it traverses through brain tissue. These measurements can then be used to calculate the regional $CMRO_2$ with good spatial and temporal resolution. Numerous assumptions are generally made such that relative changes in $CMRO_2$ are most commonly measured regionally in the cortex upon activation of neurons mapping to that cortical region (7, 8).

Different wavelengths of light have different sensitivities to oxy- and deoxyhemoglobin concentration, so one must carefully choose imaging wavelengths to ensure adequate sensitivity for the experiments in question. Extinction coefficients of oxyhemoglobin (HbO) and deoxyhemoglobin (HbR) in the mouse brain have been documented in previous studies using similar experimental conditions to this study (7). A plot of the molar extinction coefficient of

hemoglobin at various wavelengths of light is shown in Figure 1. The choice of wavelengths used to image the cortex in our study will be explained in subsequent sections.

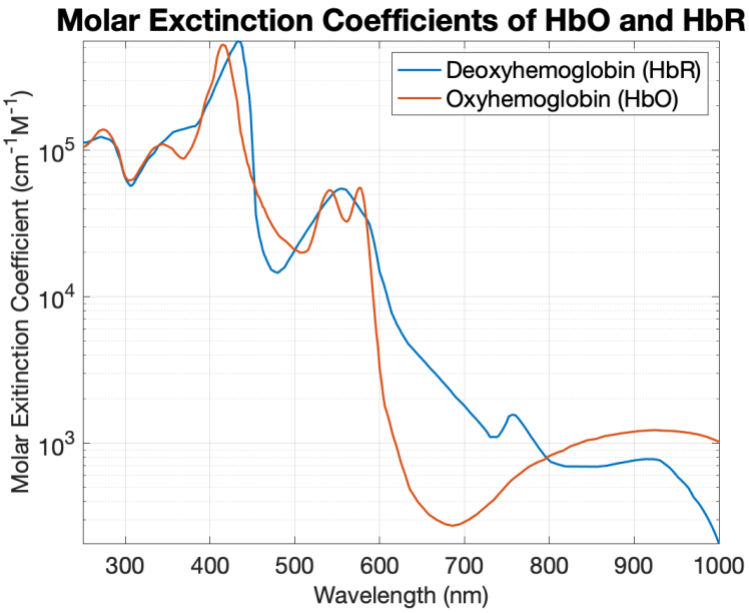

Figure 1. Extinction coefficients of hemoglobin in its fully oxygenated and deoxygenated state (oxy- and deoxy-hemoglobin, respectively) showing its light absorption properties at different wavelengths. Light between 600 and 700nm shows preferential absorption by deoxygenated hemoglobin (HbR) over oxygenated hemoglobin (HbO). These values were obtained from Ma et. al. (7).

1.3 Targeting Specific Neuronal Populations

To measure metabolism in specific neuronal populations, it is necessary to target a specific neuronal type and express proteins that enable the selective manipulation of its activity. The goal of protein insertion is to insert the deoxyribose nucleic acid (DNA) sequence for a protein into the genome of organisms. This causes the modified gene to be replicated into every cell of the offspring and the protein to be expressed throughout its lifespan. Transgenic mouse lines are created by targeting a specific DNA sequence to insert the desired gene. This can be done in two

methods: by using sophisticated targeting strategies like design and delivery of bacterial artificial chromosomes (BACs), or through random insertion of DNA plasmids early in development.

1.3.1 Random Insertion

Random insertion transgenic lines are created by introducing DNA plasmid sequences into the cell nucleus. To establish cellular specificity, these DNA sequences have promoter sequences that encode for cell-specific information regarding the cell's identity (e.g. neuron, muscle), protein localization (e.g. transmembrane, cytosol), and other cell-specific functions. It is well-known that multiple genes can share the same promoter, and as a result, a promoter can insert the desired sequence on different loci in the genome. Each locus where the desired protein sequence is placed is called a founder line. Each founder line may have different amounts of protein expression and locations of expression, and it is therefore required to assess each founder line for the desired expression prior to use.

1.3.2 Targeted Transgenic Lines

Unlike random insertion in the genome, targeted transgenic lines tend to create a more predictable and uniform expression among offspring. To create targeted transgenic mouse lines, a specific locus in the genome of the offspring is targeted for insertion of the gene. These targeted transgenic lines are often created after observing the expression in random insertion and checking gene sequences in founder lines to have acceptable sequences and the desired expression. However, a drawback of these lines is that they are more difficult to generate, making them less widely available.

1.3.3 Cre-recombinase

With the surge in targeted transgenic lines for use in different fields of investigation, cre-recombinase transgenic mouse lines were created to allow investigators to insert different sequences in the genome of the animals. Recombinases are enzymes which can "swap" sequences at specific locations in the genome. Cre-recombinase is a 38 kD protein which recognizes a 34bp sequences called *loxP* (9). Cre-recombinase binds to the *loxP* site, and when two bound cre-recombinase molecules come together, they form a tetramer along with the 2 strands of DNA bound to each enzyme. The recombinases then cut the sequences downstream from the *loxP* site and exchange the two sequences. If a virus delivers the sequence we would like to incorporate into the genome of cells in an organ, the cre-recombinase model can be used to insert the sequence into the genome. In this fashion, mice expressing cre-recombinase in a target of interest (e.g. specific cells) can be used to insert any genetic sequence that recognizes the cre "tag" into those locations through breeding or viral delivery strategies. We use several of these transgenic mouse models in our experiments.

1.4 Modulating Neurons Using Optogenetics

Examining the stimulation response of specific neuronal sub-types is possible using optogenetics. Optogenetics is a technique where proteins encoding light-sensitive ion channels are genetically inserted into the cell membrane of specific neuronal populations (10). Neuronal firing occurs as action potentials are propagated along the axons of neurons. Ion channels allow for an influx of sodium ions across the neuron's membrane, creating a voltage differential that propagates

down the axon of the neuron. Therefore, a neuronal action potential can be generated by embedding ion channels which open under certain conditions in the membrane of specific neurons. In this study we used Channelrhodopsin-2 (ChR2), a non-selective cation channel opened by illumination with blue light (450-490nm). ChR2 is a transmembrane ion-channel protein consisting of 7 alpha-helices, obtained from a unicellular green algae organism (11).

ChR2 can be trans-genetically inserted in the genome of mice to target specific neurons. After insertion, only the specific population of targeted neurons will express the ChR2 protein. As a result, when the cortex is illuminated with blue light, neurons expressing ChR2 increase their action potential firing rate. This will result in increases in electrical and metabolic activity in this population of neurons. Wang et al. characterized the response of ChR2(+) neurons in mouse cortex (10). Figure 2 shows that the extent of depolarization of ChR2(+) neurons depends upon the light stimulation duration. Panel B of the same figure shows that ChR2(-) neurons do not depolarize in the presence of the same light. Wang also reported that depolarization extent also changes with the intensity of light, and that ChR2(+) neurons depolarize rapidly after light stimulation, with a mean latency of 6.1ms (10).

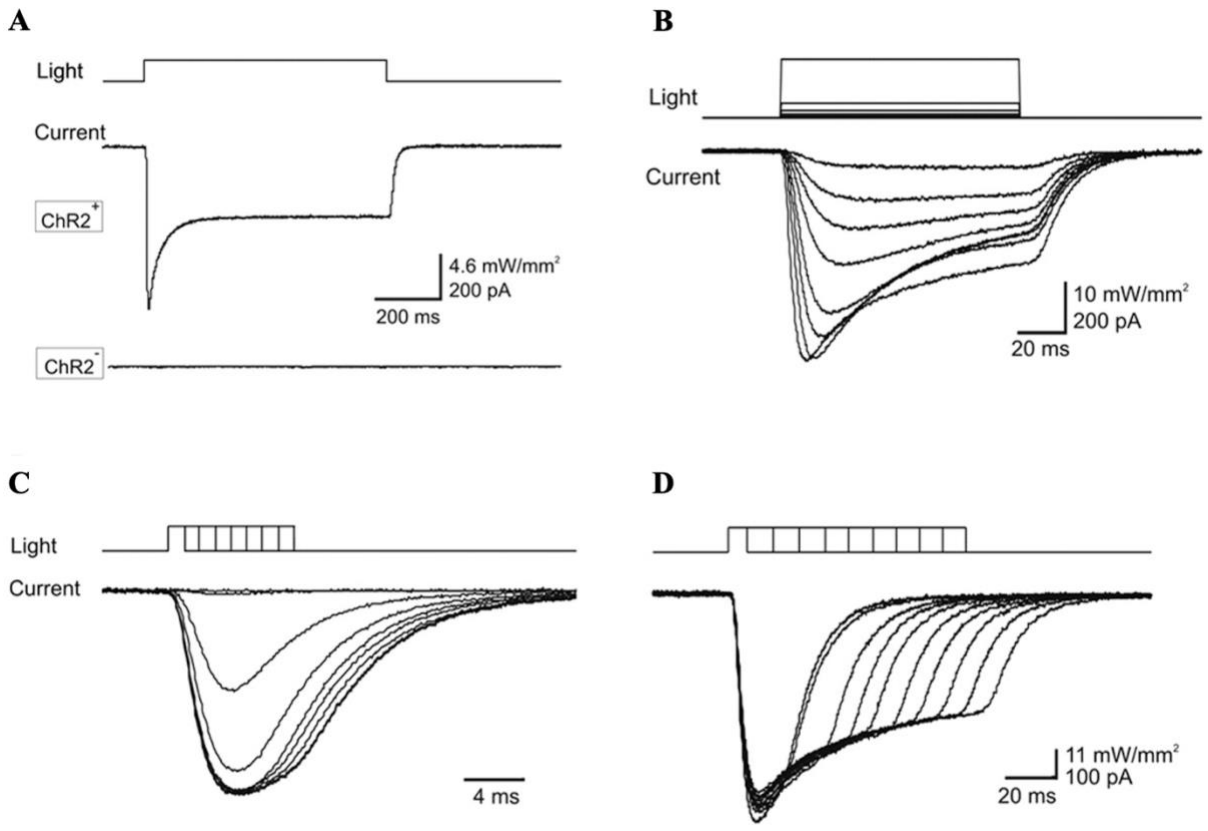

Figure 2. The response of ChR2(+) neurons in the mouse cortex. Panel (A) shows that ChR2(+) neurons depolarize upon stimulation by light, however ChR2(-) neurons do not. Panel (B) shows that stimulation with different intensities of light cause different magnitudes of depolarization in ChR2(+) neurons. Panel (C) shows that different frequencies of stimulation by light pulses cause different magnitudes of depolarization in ChR2(+) neurons. Panel (D) shows that different durations of stimulation by light cause different length of depolarizations in ChR2(+) neurons (from Wang et al. (2007)). Copyright 2007 National Academy of Sciences.

Additionally, a fluorescent reporter protein is commonly attached to ChR2. This reporter protein aids in determining the amount of ChR2 expressed in cells over different regions of the brain. In the experiments presented in subsequent sections, the ChR2 we used was fused with yellow fluorescent protein (YFP) as the reporter protein. YFP emits light in the yellow-green

wavelengths when illuminated by blue light. The blue light illumination used to open ChR2 will also excites YFP, introducing some artifacts into the optical imaging signal. The emission and absorption spectrum of YFP is shown below, as well as the absorbtion spectrum of ChR2.

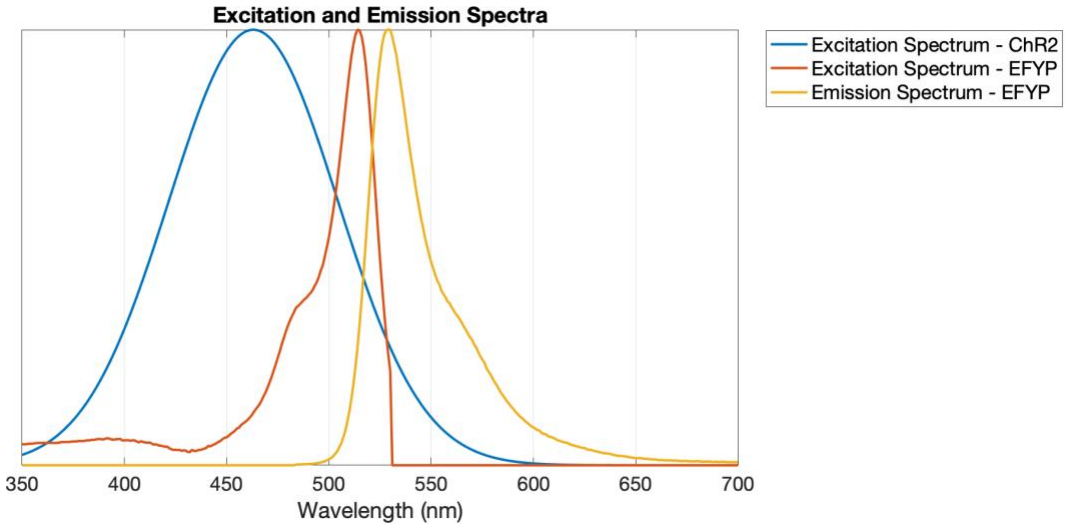

Figure 3. The absorption emission spectrum for ChR2 is shown in the blue trace. The excitation and emission spectra for EYFP are shown as the orange and yellow traces, respectively. The data to graph the spectra was obtained from the Fluorescent Protein Database (FPbase.org).

1.5 Blocking post-synaptic transmission using pharmacology

Optogenetic activation of neurons provides a powerful tool of eliciting activity in tissue composed of a heterogenous mix of neurons. However, neurons form inter-connected networks such that activation of one neuron can in-turn activate its connected post-synaptic partners. In this manner, optogenetic activation only controls the initiation of activity, not its propagation. This is a considerable problem when targeting excitatory neurons, as their function is to activate their post-synaptically connected neurons which will work to activate other downstream excitatory and

inhibitory neurons upon stimulation. To circumvent this problem, pharmacological agents that block receptors to excitatory neurotransmitters can be used to prevent the propagation of activity beyond the optogenetically activated population. In general, cortical neurons contain three types of glutamate receptors: α-amino-3-hydroxy-5-methyl-4-isoxazolepropionic acid (AMPA), N-methyl-D-aspartate (NMDA) and kainic acid receptors (KAR). Two agents are commonly used to block glutamate receptors: 2-amino-5-phosphonovalerate (APV) and 2,3-dioxo-6-nitro-7-sulfamoyl-benzo(F)quinoxaline (NBQX). APV is commonly used to block NMDA receptors, while NBQX is used to block ionotropic glutamate receptors, such as AMPA and KAR. Together, these two agents block the majority of excitatory activity. The blockade of excitatory post-synaptic potentials then allows investigators to visualize the effects of activating specific neurons in a network. Because inhibitory neurons work to inhibit rather than induce down-stream activity, their pharmacological blockade is less critical.

1.6 Neuronal subtypes

In this study, we focus on several different neuronal subtypes based on their principal signaling neurotransmitter and genetic identity. We have chosen to use this classification strategy because it has been shown to be generally maintained across mammalian species. We examine the metabolic impact of activating excitatory pyramidal neurons (a subset of neurons in Layers 2, 3 and 5 targeted by the promoter Thy1) and most cortical inhibitory neurons (targeted by the promoter VGAT). We also further examine the potential role of sub-types of inhibitory neurons. These include parvalbumin (PV), vasointestinal peptide (VIP), somatostatin (SOM), nitric oxide synthase (NOS) and neuropeptide-Y (NPY) expressing neurons. The first three types compose the

majority of cortical inhibitory neurons with little or no overlap between these groups, while the last two types tend to also express somatostatin. We include these sub-types because they have been implicated as strong CBF regulators (12, 13). The relative quantity of each subtype of neuron in the mouse cortex is detailed in Figure 4.

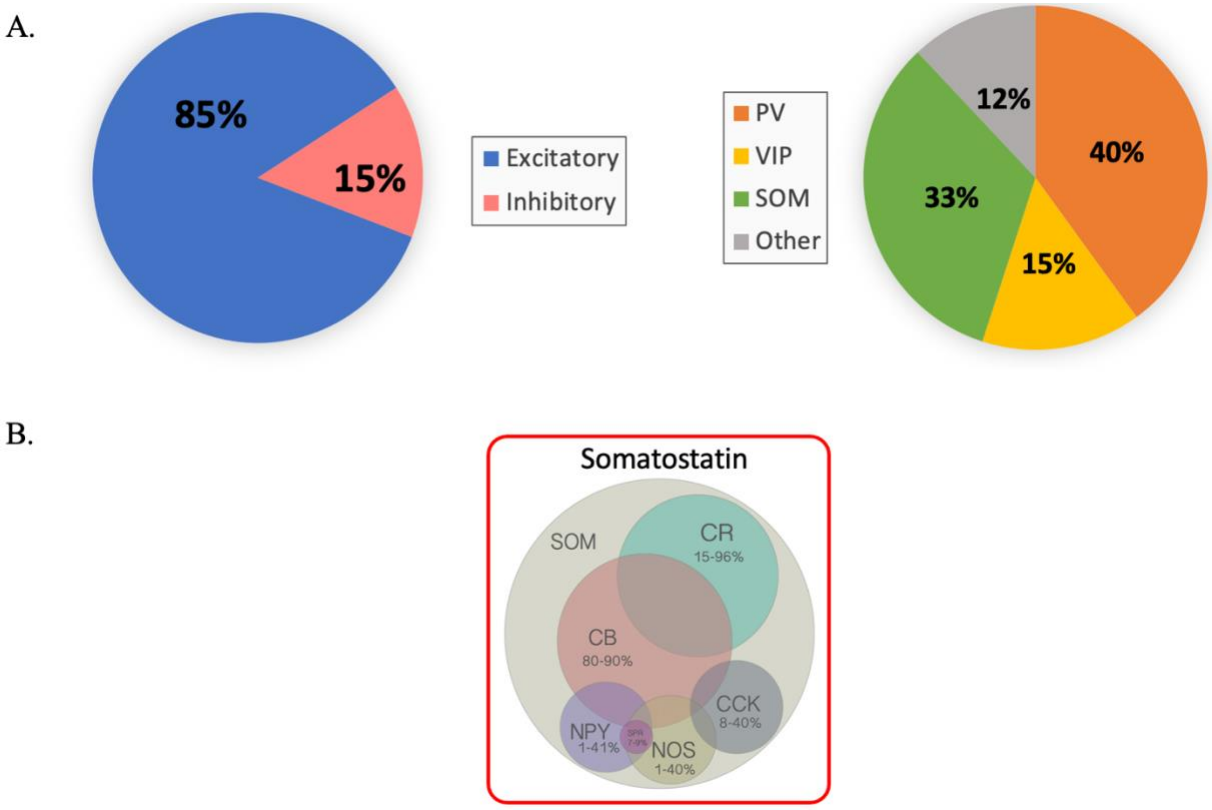

Figure 4. (A) Proportion of excitatory and inhibitory neurons in mouse cortex (left panel). Inhibitory neurons can be generally classified as those expressing PV, VIP, and SOM (right panel). Somatostatin neurons form a very diverse group of neurons with many neurons expressing other different peptides (14). Copyright 2016 Yavorska et. al.

1.6.1 Excitatory Neurons

The Thy1 gene is commonly used to target cortical pyramidal neurons, since it is expressed in the majority of pyramidal neurons in the brain. Thy1 is a cell-surface antigen, which is present in many cortical excitatory neurons. Data published by Wang et al. suggested that the largest ChR2-YFP expression occurred in layer V of the mouse cortex, where there was an even distribution of Thy1-Chr2-YFP within the layer (10). The even distribution of Thy1-ChR2-YFP neurons can be seen in a multiphoton image in Figure 5. This optogenetic model targets approximately 30-40% of all pyramidal cells in cortex. Because sensory activity initially activates excitatory neurons in primary sensory networks, we expect changes in CBF and $CMRO_2$ upon optogenetic stimulation of Thy1 neurons to be similar to those of sensory stimulation.

1.6.2 Inhibitory Neurons

A characteristic of inhibitory neurons in the brain is that they use γ-aminobutyric acid (GABA) as their neurotransmitter. As cortical inhibitory neurons synthesize the vesicular GABA transporter protein, it is a feasible protein to target to allow for the transgenic insertion of the ChR2 ion channel. Referring to this transgenic model, Zhao et al. reported that 96% of neurons which expressed the enzyme glutamic acid decarboxylase 67 (GAD-67) contained ChR2-YFP in the cortex of the VGAT-transgenic mice (15). Since GAD-67 is the enzyme in the final step of GABA synthesis, the vast majority of inhibitory neurons contain GAD-67. Thus, VGAT-ChR2-YFP has a high co-localization with inhibitory neurons in the transgenic VGAT mouse model. Additionally, Zhao et al. demonstrated that targeting VGAT resulted in an even distribution of ChR2-YFP in the

mouse cortex. The even distribution of both Thy1 and VGAT neurons in the cortex is shown in fluorescence images acquired by Wang (2007) and Zhao (2011) in Figure 5 (10, 15).

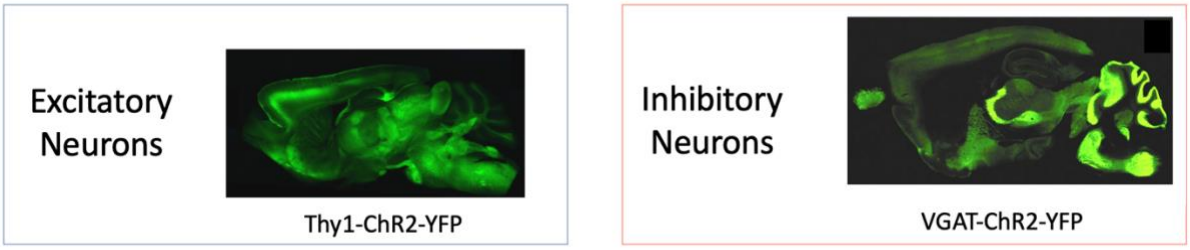

Figure 5. The distribution of Thy1-ChR2 (left) and VGAT-ChR2 in the mouse cortex (10, 15). These images show that the distribution of neurons within the cortex is even. Copyright 2007 National Academy of Sciences (left), Copyright 2011 Nature Publishing Group (right).

VGAT-targeted neurons include almost all inhibitory neurons, and thus we expect the response to optogenetic stimulation to be a combination of all of the major inhibitory subtypes. The main inhibitory subtypes are described below.

1.6.2.1 Parvalbumin (PV)

PV neurons are the most abundant inhibitory neuronal subtype, comprising 35-40% of GABAergic neurons (16). PV neurons are the strongest inhibitors of pyramidal neurons and have been implicated in the generation of gamma band activity because of their ability to spike at high frequencies (greater than 20-30 Hz). Their strong inhibitory capacity stems from their influence on the cell bodies and initial axonal segments of pyramidal neurons.

1.6.2.2 Vasointestinal peptide (VIP)

VIP is a peptide expressed or secreted by cells and it has been extensively characterized in the digestive tract. It is also expressed by 10 to 30% of all GABAergic neurons in cortex (16). The role of VIP in the brain is not clear but it provides a genetic identifier for neurons that express GABA and generally do not express PV.

1.6.2.3 Somatostatin (SOM)

SOM neurons are the second most abundant inhibitory neuronal subtype in mouse cortex, consisting 20-35% of GABAergic neurons (16). Similar to VIP, somatostatin is a peptide expressed by various cells. It has been well characterized in the pancreas, but its role in the brain is also unknown. As a genetic marker, it outlines a heterogenous population of neurons that also co-express numerous other markers (Figure 4B). Two interesting sub-populations of SOM neurons include those that also express nitric oxide synthase (NOS) and/or neuropeptide-Y (NPY). These two peptides have been implicated in dilation and constriction of nearby vasculature (12), hence our interest in examining them in this study.

1.6.2.4 Nitric oxide synthase (NOS)

Nitric oxide synthase is the enzyme that catalyzes the generation of nitric oxide (NO), a small molecule that is known to be a potent vasodilator. Different to other inhibitory neurons, NOS neurons can have longer axonal and dendritic arbors despite their lower numbers. Due to nitric oxide's strong ability to dilate vessels, the axons of the majority of NOS neurons appear to target the microvasculature, thus supporting the fact that NOS neurons are important in regulating blood flow for neuronal circuits (17).

1.6.2.5 Neuropeptide-Y (NPY)

NPY is a subtype of GABAergic neurons that also express SOM, and make up about 8% of inhibitory neurons in the brain (16). NPY neurons have been reported to play a large role in stimulating mammalian food intake (18).

1.7 Other Work

The majority of studies assessing the cerebral metabolic rate of oxygen consumption ($CMRO_2$) of specific neuronal populations have been conducted in anesthetized animals. By design, anesthetics act to suppress neuronal activity and, therefore, do not provide a clear understanding of brain metabolism in the awake state. In 2005, Dunn et al reported $CMRO_2$ upon forepaw and whisker stimulation in awake rodents using optical imaging techniques (8). Stimulation of sensory systems such as vision and somato-sensation, however, indiscriminately activates many different neurons in the brain and it becomes very difficult to isolate metabolic responses to a subset of neurons. Subsequent studies have used optogenetic techniques to separately stimulate subsets of excitatory or inhibitory neurons and examine the $CMRO_2$ response in the mouse cortex (2-4).

In 2021, Lee et. al., aimed to examine the PV neuron contribution to local $CMRO_2$, blood flow, and blood volume changes. These experiments were conducted in awake mice, and the group compared the PV response to the Thy1 response in the same experimental condition. They found that $CMRO_2$ increased by 3.46% in Thy1-ChR2 animals and decreased by 1.84% in PV-ChR2 animals (3). Since there was a local decrease in oxygen consumption and cerebral blood flow, the authors conclude that the effect of inhibition is observed. The inhibitory effect on excitatory

neurons makes it difficult to ascertain PV oxygen consumption relative to excitatory neuron activity. Additionally, the lack of change in blood flow suggests that PV neurons do not have a strong influence on blood flow changes.

Another group, Dahlqvis et al. (2020), aimed to determine the driving force behind the $CMRO_2$ response. This study was done in anesthetized animals. They used CAMKIIα-ChR2 to target a larger set of excitatory pyramidal neurons, and PV-ChR2 to target a subset of inhibitory neurons. Upon optogenetic activation, the excitatory neurons had a $CMRO_2$ increase of 19%, while the PV neurons had an increase in $CMRO_2$ of 5% (2). These results differ from those of Lee et al. as no decrease of $CMRO_2$ is observed upon optogenetic stimulation of the PV neurons.

Our group previously measured $CMRO_2$ in anesthetized Thy1-ChR2 as well as VGAT-ChR2 animals to compare the differences in oxygen metabolism. We reported an increase in $CMRO_2$ of +1.5% after optogenetic stimulation in excitatory neurons, and a decrease in $CMRO_2$ of -1.5% after optogenetic stimulation of inhibitory neurons (4). Thus, the effect of local inhibition upon VGAT optogenetic stimulation was observed. Moreover, after blocking NMDA and AMPA receptors with APV and NBQX, the $CMRO_2$ of VGAT-ChR2 animals became +3.9% upon optogenetic stimulation, suggesting that inhibitory neurons have a higher rate of oxygen metabolism than do excitatory neurons (4).

The aforementioned studies vary widely in their findings and comparisons of excitatory and inhibitory neuron oxygen metabolism, which is likely due to different experimental conditions. Additionally, these studies did not consider the difference in the number of neurons activated by excitatory and inhibitory neuron stimulation. It is known that excitatory neurons vastly outweigh inhibitory neurons in the cortex, so this difference should be accounted for in the comparison between excitatory and inhibitory neuronal $CMRO_2$ changes. In this work, we examine $CMRO_2$

in awake mice and extract a metric related to the number of targeted neurons in an attempt to normalize the $CMRO_2$ by the number of neurons activated. Additionally, we will use the same experimental conditions previously used by our group and compare our results with those published in anesthetized mice to determine if there is a difference in oxygen consumption between neuronal subtypes. Given the findings of previous work, we expect to see a greater change in local $CMRO_2$ upon optogenetic stimulation of inhibitory neurons.

We will also investigate cell-specific responses as part of this work. Previous studies have suggested that PV neurons are unable to regulate cerebral blood flow, but consume significant amounts of oxygen (2, 3, 12). We therefore might expect a minimal contribution to cerebral blood flow and an increase in oxygen metabolism upon optogenetic stimulation of PV neurons. On the other extreme, it is known that NOS neurons are strong regulators of blood flow (12). Thus, we might expect to see a marked increase in cerebral blood flow but little change in oxygen metabolism upon optogenetic stimulation of NOS neurons, given their low numbers. Finally, our lab has shown that VIP neurons have limited effect on cerebral blood flow in anesthetized mice (12), so we consequently might expect to see limited increases in both blood flow as well as oxygen metabolism upon optogenetic stimulation of VIP neurons.

2.0 Calculating $CMRO_2$

2.1 $CMRO_2$ Model

$CMRO_2$ is the metric used to report the oxygen consumption rate in a region of tissue with units of mol/min. Fick's principle states that the rate of oxygen consumption in tissue ($CMRO_2$) is the difference between the rate of oxygen entering the tissue minus the rate of oxygen leaving the tissue (Eq. 1).

$$\mathrm{CMRO_2} = \mathrm{CBF}(\mathrm{C_a} - \mathrm{C_v}) \quad (1)$$

In this expression CBF is the cerebral blood flow with units of mL/min, C_a is the concentration of arterial blood oxygen (entering the sampled region), and C_v is the concentration of venous blood oxygen (exiting the sampled region), both with units of moles/mL. A depiction of the model used to interpret neuronal oxygen consumption is presented in Figure 6.

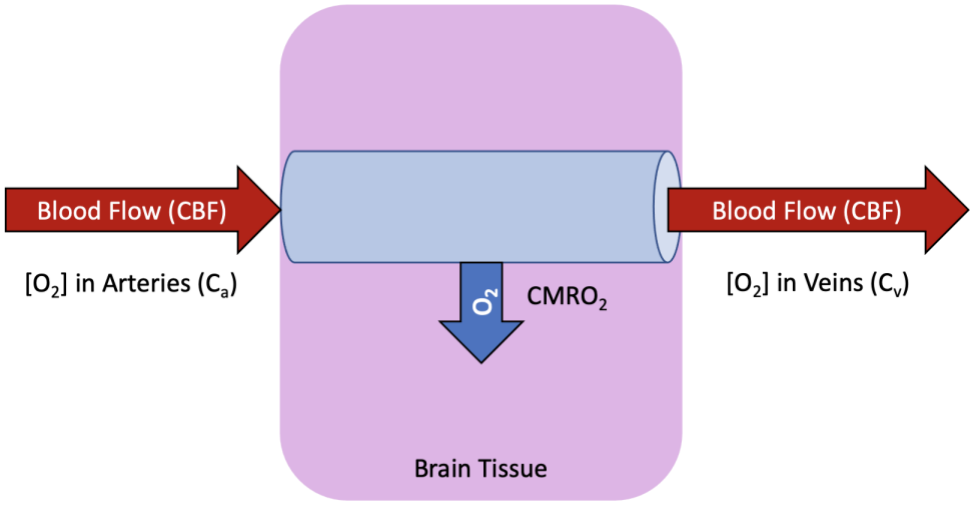

Figure 6. Depiction of Fick's principle to calculate $CMRO_2$ as used in this study.

We can define the oxygen extraction fraction (OEF) as:

$$\mathrm{OEF} = \frac{C_a - C_v}{C_a} \tag{2}$$

Given this definition of OEF, we can rewrite the $CRMO_2$ equation as:

$$\mathrm{CMRO_2} = \mathrm{CBF} \cdot C_a \cdot \mathrm{OEF} \tag{3}$$

Common systems to measure CBF can do so in relative units (using a baseline period of interest), although absolute measurements are possible with several trade-offs. Similarly, absolute measurements of oxygen content using optical methods are difficult to obtain, but relative changes can be extracted when control or baseline periods can be identified. Hence, we can rewrite $CMRO_2$ as the relative change in $CMRO_2$ as follows:

$$\mathrm{rCMRO_2} = \frac{\mathrm{CBF_1} \cdot C_{a,1} \cdot \mathrm{OEF_1}}{\mathrm{CBF_0} \cdot C_{a,0} \cdot \mathrm{OEF_0}}, \tag{4}$$

where measurements are taken both before (subscript ",0") and after a perturbation (subscript ",1"). In our model, we consider arteries to deliver fully oxygenated blood such that the oxygenation at the input does not change and remains constant, making the ratio $\frac{C_{a,1}}{C_{a,0}} = 1$. Additionally, the term $\frac{\mathrm{CBF_1}}{\mathrm{CBF_0}}$ can be written as rCBF, denoting a ratio of CBF between two conditions.

To further simplify the model, we can consider that the great majority of oxygen in the blood is carried by hemoglobin (98%). We can rewrite OEF using the concentration of fully oxygenated (C_{HbO}), fully deoxygenated (or reduced, C_{HbR}) and total hemoglobin ($C_{HbT} = C_{HbO} + C_{HbR}$) as:

$$\mathrm{OEF} = \frac{C_{HbR}}{C_{HbT}}, \tag{5}$$

Combining Eq. 4 and Eq. 5, simplifying the term $\frac{\mathrm{OEF}_2}{\mathrm{OEF}_1}$, and using the convention that $\Delta C_X = C_{X,2} - C_{X,1}$, we obtain the equation,

$$\mathrm{rCMRO}_2 = \mathrm{rCBF}\frac{1+\frac{\Delta C_{\mathrm{HbR}}}{C_{\mathrm{HbR},0}}}{1+\frac{\Delta C_{\mathrm{HbT}}}{C_{\mathrm{HbT},0}}}. \quad (6)$$

2.2 Model assumptions

The model proposed in section 2.1 makes several assumptions about the underlying physiology in the brain. The first is that all O_2 is carried by hemoglobin. The second assumption is that arterial blood (the blood coming into the region for $rCMRO_2$ to be calculated in), is fully oxygenated (arterial saturation is 100%). Third, this model assumes that oxygen delivery and consumption are in continuous equilibrium (steady state). This implies that for every observation oxygen extracted from hemoglobin is consumed in tissue. Additionally, we assume values for the initial concentration of oxyhemoglobin of 60µM, and deoxyhemoglobin of 40µM (8).

2.3 Modified Beer-Lambert's Law

To compute $rCMRO_2$ according to Eq. 6, the change in concentration of C_{HbR} as well as that of C_{HbT} must be known. If we image the cortex at two wavelengths sensitive to change in hemoglobin levels, we are able to solve for the two unknowns using Beer Lambert's law. Beer Lambert's law states that

$$I = I_0 e^{-\mu_a X}, \quad (7)$$

where I is the reflectance at one wavelength, and I_0 is the reflectance at the same wavelength measured before perturbation. μ_a is the absorption coefficient of material a, where the light travels the pathlength X (7). In the case of our model, the matter of interest is hemoglobin, which we can attribute to a combination of oxyhemoglobin (HbO) as well as deoxyhemoglobin (HbR), modifying (Eq 7.) to be:

$$I = I_0 e^{(-\mu_{CHbO} - \mu_{CHbR})X}. \tag{8}$$

Since pathlength is only wavelength dependent, HbO and HbR can be multiplied by the constant pathlength. The absorption coefficient μ can be defined as:

$$\mu_a = \epsilon_a \Delta C_a \, , \tag{9}$$

where ϵ is the extinction coefficient of chromophore a, and ΔC is the change in concentration relative to a baseline period of chromophore a. So that the changes in concentrations of our chromophores of interest, HbR and HbO can be measured, we take the natural log of both sides of beer lambert's law. After simplification, this results in the equation:

$$\Delta A(\lambda, \, t) = \left(\epsilon_{HbO}(\lambda)\Delta C_{HbO}(t) + \epsilon_{HbR}(\lambda)\Delta C_{HbR}(t)\right)D(\lambda) \, , \tag{10}$$

where ΔA is defined as $-\ln\left(\frac{I}{I_0}\right)$, as recorded by the imaging system at a wavelength (λ), and D is the differential pathlength factor at a wavelength, which also takes into account the scattering of light as it travels through the cortex (8). The values for the extinction coefficients as well as the pathlength factor have been reported in the literature, and we obtained them from Ma et. al., who reported and used these values in mouse cortex (7).

To solve for the change concentrations of HbO and HbR, we can image at two different wavelengths, then solve the system of equations:

$$\begin{bmatrix} \Delta A(\lambda_1, \, t) \\ \Delta A(\lambda_2, \, t) \end{bmatrix} = \begin{bmatrix} \epsilon_{\mathrm{HbO}}(\lambda_1)D(\lambda_1) & \epsilon_{\mathrm{HbR}}(\lambda_1)D(\lambda_1) \\ \epsilon_{\mathrm{HbO}}(\lambda_2)D(\lambda_2) & \epsilon_{\mathrm{HbR}}(\lambda_2)D(\lambda_2) \end{bmatrix} \cdot \begin{bmatrix} \Delta C_{\mathrm{HbO}}(t) \\ \Delta C_{\mathrm{HbR}}(t) \end{bmatrix}. \tag{11}$$

Once we have calculated ΔC_{HbO} and ΔC_{HbR}, ΔC_{HbT} is related such that

$$\Delta C_{\mathrm{HbT}}(t) = \Delta C_{\mathrm{HbR}}(t) + \Delta C_{\mathrm{HbO}}(t)\ . \tag{12}$$

2.4 Calculating $CMRO_2$ using optical imaging data at multiple wavelengths

Eq. 6 can be used to compute the $CMRO_2$ provided with blood flow data as well as oxygenation-sensitive optical imaging data at least two wavelengths. Blood flow data, especially relative measurements (rCBF), can be obtained using methods that are compatible with optical imaging such as laser Doppler flowmetry (LDF). In 2005, Dunn et al. proposed a slight modification to the formula as:

$$\mathrm{rCMRO_2} = \mathrm{rCBF}\frac{1+\gamma_r\frac{\Delta C_{\mathrm{HbR}}}{C_{\mathrm{HbR},0}}}{1+\gamma_t\frac{\Delta C_{\mathrm{HbT}}}{C_{\mathrm{HbT},0}}}, \tag{13}$$

where γ_r and γ_t are vascular weighting constants (8). These constants account for the potential variations in the amount of HbR and HbT between regions or volumes of interest. In this work we rely on a single large brain region such the values in the regions of interest are assumed to not vary a substantial amount.

2.5 Calculating $CMRO_2$ using optical imaging at a single wavelength

Motivated by the magnetic resonance imaging (MRI) method of computing $CMRO_2$,we set out to derive a similar model for optical imaging using the same framework previously mentioned. In MRI, arterial spin labeling (ASL) and blood-oxygenation level dependent (BOLD)

MRI signals are used as measurements of changes in blood flow and blood oxygenation, respectively. MRI and optical methods can be designed to share very similar sensitivities where ASL is similar to obtaining blood flow measurements via laser doppler flowmetry (or several other methods including speckle contrast), and BOLD imaging is analogous to imaging at HbR-weighted wavelengths (e.g. 620nm). To facilitate calculation at one wavelength, Eq. 6 can be modified given that an empirical relationship exists between rC_{HbT} and rCBF. This model would only require deoxygenated hemoglobin sensitive wavelength and would not be subject to differences in light pathlengths from multiple wavelength illumination.

In 1974, Grubb et al. proposed that a power law can be used to describe the relationship between cerebral blood flow and cerebral blood volume in the brain (19). The relationship can be expressed by the formula:

$$\mathrm{rCBF} = \mathrm{rCBV}^{\alpha} . \tag{14}$$

Since the optical measure of blood volume can be reasonably approximated by the total amount of hemoglobin in a measurement volume, we can assume that $\mathrm{rCBV} \approx \mathrm{rC_{HbT}}$. The exponent α has been experimentally determined to be between 0.2 and 0.25 in mice (8). It is important to note, that this relationship also implies a steady state between blood flow and volume.

Combining and simplifying Eq. 6, Eq. 10, and Eq. 14 yields the equation for computing $rCMRO_2$ from one wavelength optical imaging data (Eq. 15). In this expression, $\Delta A = (-\ln(\frac{I(t)}{I_0})$ is the change in optical signal weighted to deoxygenated hemoglobin.

$$\mathrm{rCMRO_2} = \mathrm{rCBF}^{1-\alpha}(1 + \beta\Delta\mathrm{A}) \tag{15}$$

β is a calibration factor and contains the terms $\beta = \frac{1}{D\epsilon_{HbR}C_{HbR,0}}$ and provides a rough magnitude for this coefficient. Once β is known, Eq. 15 only requires blood flow data and one wavelength of imaging data.

2.6 Calibrating single wavelength $CMRO_2$ model

The one-wavelength model needs to be calibrated to find the coefficient β to enable the calculation of $rCMRO_2$. To determine this coefficient, a condition must be found where $rCMRO_2$, rCBF and ΔA are known. This condition can be accomplished with measurements of rCBF and ΔA during the delivery of low-grade hypercapnia (e.g. 5% CO_2 in air) which produces a systemic increase in blood flow without causing changes oxygen metabolism ($rCMRO_2 = 1$) (20, 21). Thus, knowing $rCMRO_2$, rCBF, and ΔA, we can solve for the calibration factor β from Eq. 15 as follows:

$$\beta = \frac{\mathrm{rCBF}^{\alpha-1}-1}{\Delta A}. \tag{16}$$

2.7 Simulation

To provide a more intuitive understanding of the calculation of $CMRO_2$ and the impact of different physiological changes, simulations with different CBF, $CMRO_2$ and OIS changes were conducted to illustrate their effect on the acquired data and provide a sense for their effect size. With our imaging setup, we measure rCBF using laser Doppler flowmetry (LDF), and compute rC_{HbT} and rC_{HbR} using an optical imaging system (OIS) at two different wavelengths: 570nm and 620nm. The imaging setup will be described in more detail in section 3.2.

We simulate three scenarios: (1) Increase in CBF without change in $CMRO_2$, (2) Increase in $CMRO_2$ without change in CBF, (3) Changes in both CBF and $CMRO_2$. We also simulate a scenario where only the OIS 620 signal changes to inspect its effects on $rCMRO_2$. For these different scenarios we used changes in CBF, OIS 570 and OIS 620 of +20%, -1% and +0.3%, respectively, which are typically observed in our laboratory from sensory stimulation studies . To

mimic the data we present in the results, these signal changes are presented as time series with the change captured by a bump in the time series using raised cosine or gamma functions.

2.7.1 No change in $rCMRO_2$ with changes in rCBF

In the first simulation, we observe the changes necessary to maintain $rCMRO_2 = 1$ (i.e. 0% change) while changing CBF by 20%. Using Grubb's relationship ($\alpha = 0.25$) we can get a reasonable estimate for rC_{HbT} (+4.6%) and this allows us to solve for the necessary rC_{HbR} (-12.8%), OIS 570 (-0.7%) and OIS 620 (+1.3%) signals that meet $rCMRO_2 = 1$ (Figure 7). This simulation is inspired by our interest in investigating calibration of $rCMRO_2$ measurements using CO_2. Since CO_2 is a vasodilator, we expect blood flow as well as blood volume increases. This simulation shows that to keep $rCMRO_2$ constant while changing rCBF, rC_{HbT}, and rC_{HbR}, the OIS 620 signal must increase by a significant amount compared to sensory stimulation.

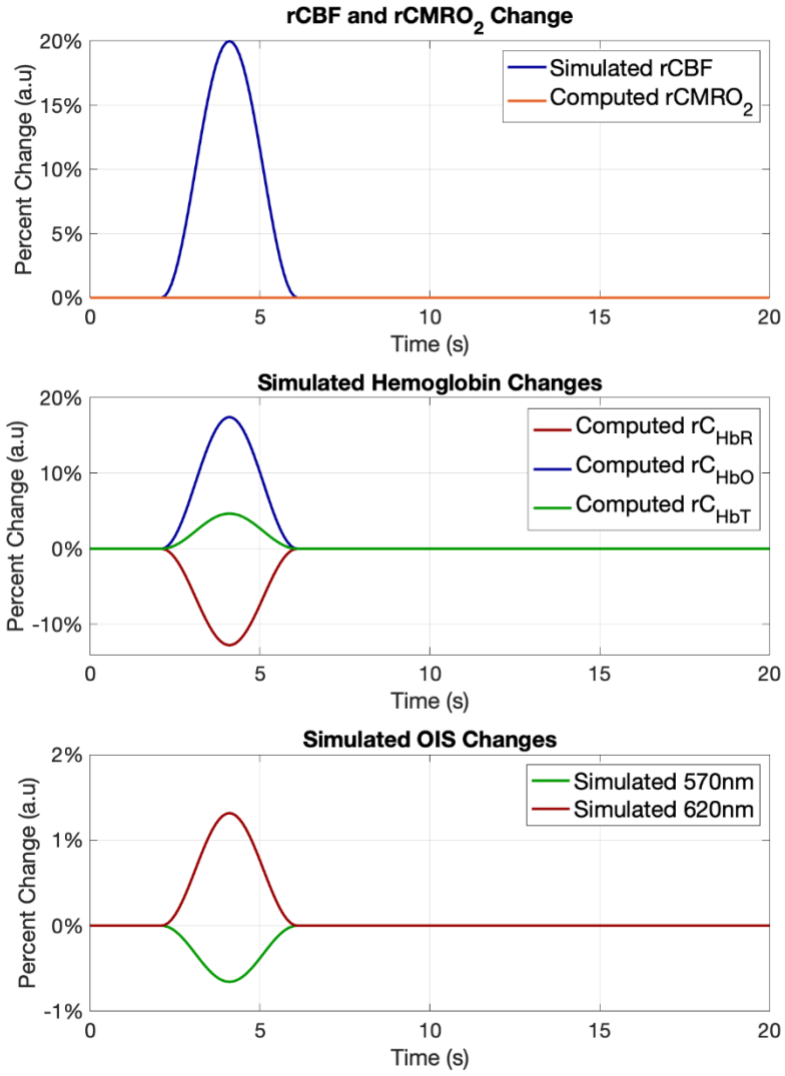

Figure 7. Simulated physiological conditions, forcing $rCMRO_2$ to not change, while changing all other variables. rC_{HbR} and rC_{HbT} were computed using modified Beer Lambert's law (Eq. 11). $rCMRO_2$ was computed using the 2-wavelength model from Eq. 6.

2.7.2 No change in rCBF with changes in $rCMRO_2$

The inherent relationship between rCBF and rC_{HbT} in Eq. 14 shows that when rCBF does not change, neither does rC_{HbT}. Under these conditions, changes in OIS 570 of 0% and OIS 620 of -0.8% produce increases in $CMRO_2$ of +5%. Larger negative changes in OIS 620 would produce even larger increases in $CMRO_2$. In other words, for $rCMRO_2$ to increase in the absence of blood flow changes, the concentration of HbR must increase, rather than the normal decrease we normally observe with sensory stimulation. This makes sense physiologically, as this suggests that in the absence of blood flow, there is an accumulation of deoxy-hemoglobin in the brain in the oxygen-consuming region. Graphs showing these changes are shown below in Figure 8.

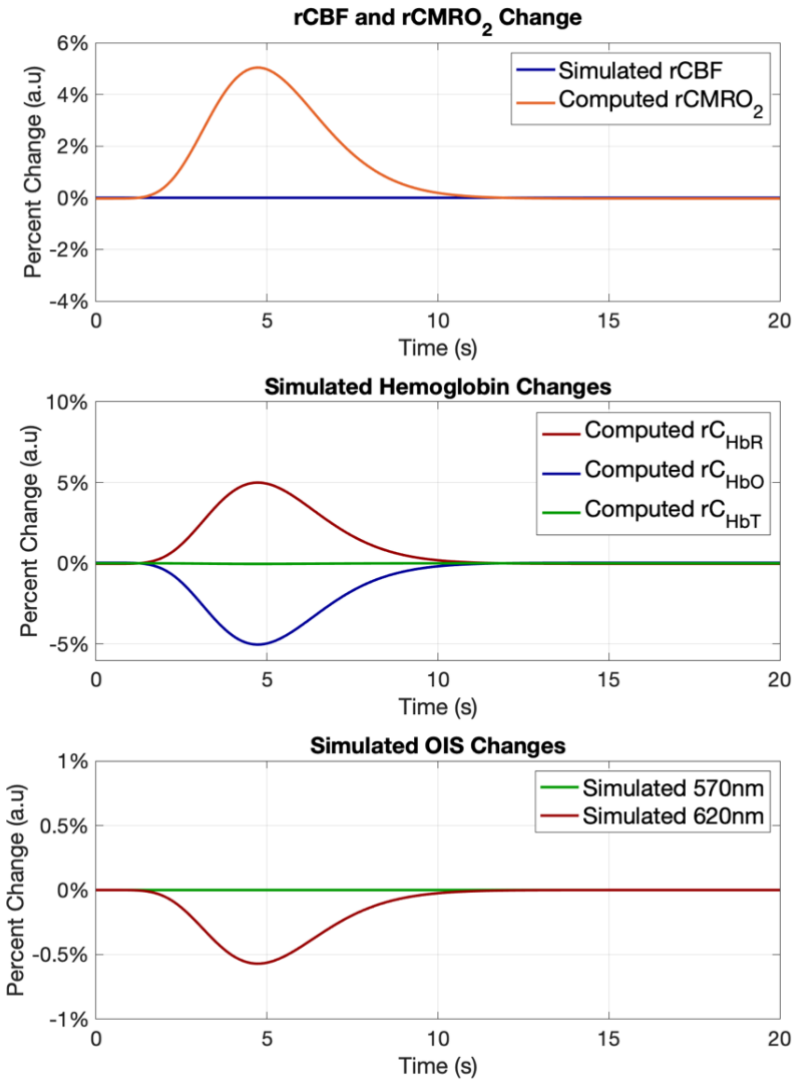

Figure 8. Simulated physiological conditions, forcing $rCMRO_2$ peak at 5%, while not changing rCBF. rC_{HbR} and rC_{HbT} were computed using modified Beer Lambert's law (Eq. 11). $rCMRO_2$ was computed using the 2-wavelength model from Eq. 6.

2.7.3 Changes in rCBF and $rCMRO_2$

In this scenario we simulate increases in CBF of +20% with increases in $CMRO_2$ of +10%. As done for scenario 1, we used Grubb's relationship to obtain an estimate of rC_{HbT} of +4.6%, as before, and use this to solve for the necessary rC_{HbR} (-4.0%), OIS 570 (-0.7%) and OIS 620 (+0.3%) signals which met a $CMRO_2$ increase of +10% ($rCMRO_2$ = 1.1). Graphs showing these changes are shown below in Figure 9.

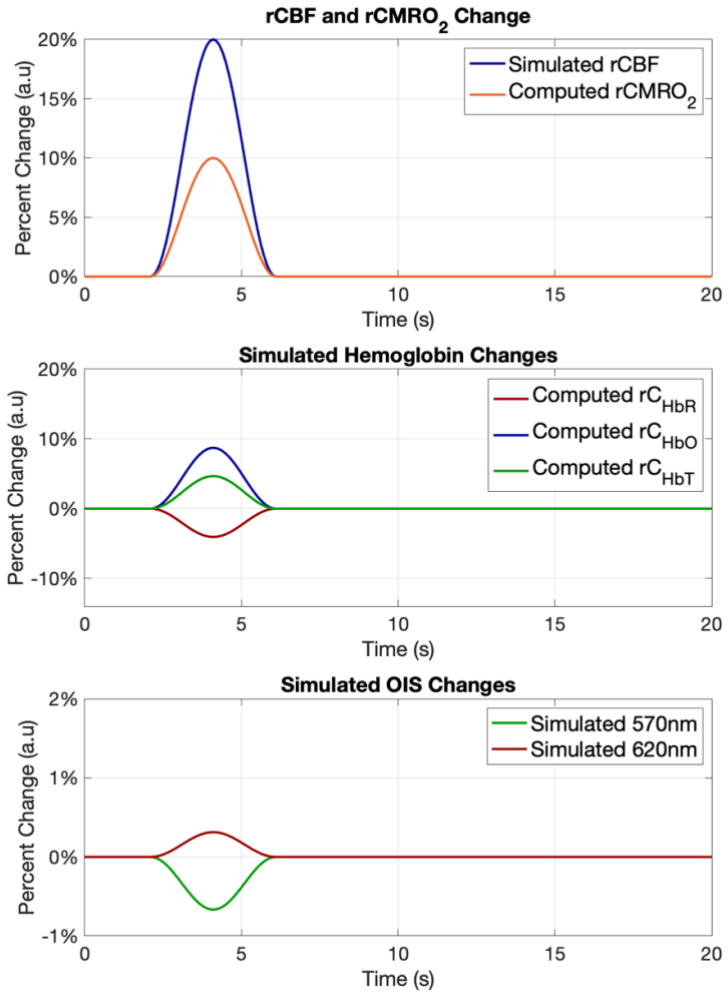

Figure 9. Simulated physiological conditions, forcing $rCMRO_2$ to increase by 10%, and rCBF by 20%. rC_{HbT} was computed using Grubb's relation, and rC_{HbR} was computed using modified Beer Lambert's law (Eq. 11). $rCMRO_2$ was computed using the 2-wavelength model from Eq. 6.

The goal of this simulation was to give our model CBF and $CMRO_2$ changes over a range typically reported for sensory responses in cortex and observe the magnitude of the OIS signals computed. Interestingly, to obtain larger increases in $CMRO_2$ for the same increase in CBF, decreases in the OIS 620nm signal are necessary (e.g. OIS 620nm changes of -0.5% would produce $CMRO_2$ increases of 20%).

2.7.4 Change in OIS 620 signal alone

The purpose of the final simulation was to explore the effects of the change in OIS 620 signal on $CMRO_2$. The previous simulations showed that changes in OIS 570 relate to changes in C_{HbT} and CBF, and that decreases in OIS 620 relate to increases in $CMRO_2$. In this simulation, we explore the magnitude of changes on 620nm signal without changes in CBF. An increase in OIS 620 signal of +0.3% produced changes in rC_{HbT} and rC_{HbR} of 0.02% and -2.62%, and the resulting change in $rCMRO_2$ was -2.62%. Graphs showing these changes are shown below in Figure 10.

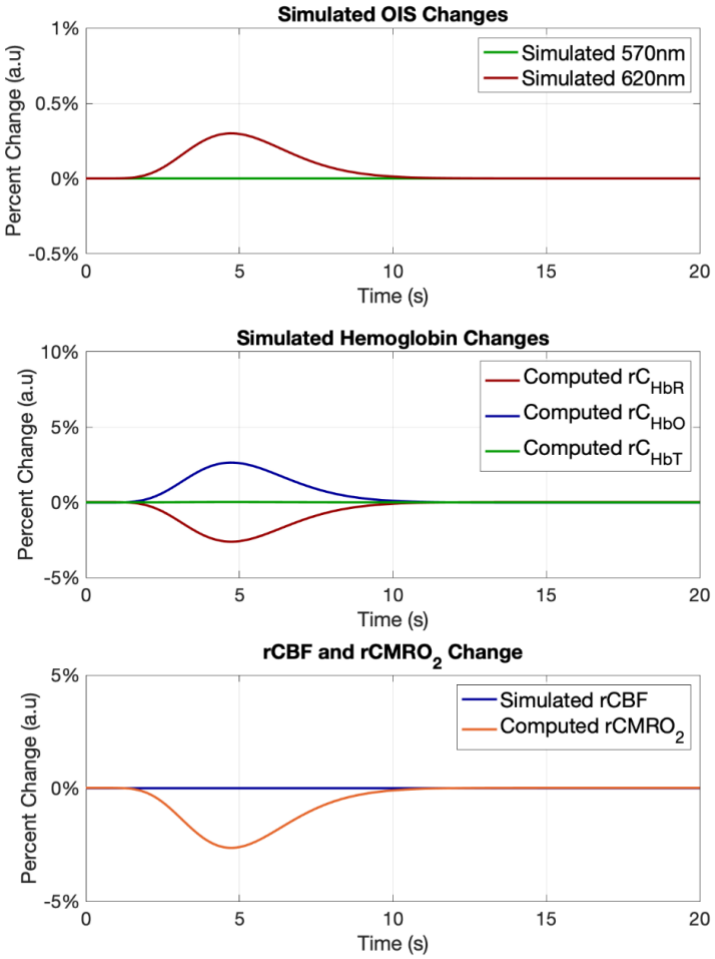

Figure 10. Simulated physiological conditions, forcing LDF and OIS 570 to not change, however changing OIS 620. rC_{HbR} and rC_{HbT} were computed using modified Beer Lambert's law (Eq. 11). $rCMRO_2$ was computed using the 2-wavelength model from Eq. 6.

This simulation suggests that in the absence of a blood flow and blood volume change, rC_{HbR} must increase, rather than the decrease we normally see following sensory stimulation. From this, we can conclude that the OIS 620 signal must be negative in deflection to suggest an increase in $rCMRO_2$. This simulation is of interest, because it is thought that those select subtypes of neurons do not regulate blood flow, however, still have a metabolic footprint. Upon stimulation of

these neurons, according to this simulation, we would expect to see a decrease in the OIS 620 signal, as opposed to the increase we normally notice upon somatosensory stimulation.

3.0 Methods

3.1 Animal Preparation

A total of 23 mice (male; 23 to 32g; 3 to 9 months old) were obtained from Jackson Laboratories (Bar Harbor, ME). For the first set of optogenetic experiments, transgenic mice expressing ChR2 fused with YFP in excitatory neurons (Thy1-ChR2-YFP; *n*=3, strain B6.Cg-Tg(Thy1-COP4/EYFP)18Gfng/J) and inhibitory neurons (VGAT-ChR2-EYFP, *n*=2 strain B6.Cg-Tg(Slc32a1-COP4*H134R/EYFP)8Gfng/J) were used (10, 15). For the second set of optogenetic experiments, the cre-recombinase model system targeted to specific sub-populations of inhibitory neurons was used to selectively express the same optogenetic protein (ChR2 fused with YFP) into these cells. The following neuronal targets and mice were used for this portion of the study in a total of 18 mice: PV (PV-cre, *n*=3, strain B6.129P2-Pv(albtm1(cre)Arbr)/J), VIP (VIP-cre, *n*=2 strain VIP(tm1(cre)Zjh)/J), SOM (SOM-cre, *n*=5 strain B6N.Cg-SST(tm2.1(cre)Zjh]/J), NOS (NOS-cre, $n = 4$ strain B6.129S-Nos1(tm1.1(cre/ERT2)Zjh)/J), and NPY (NPY-cre, *n*=4 strain B6.Cg-Npytm1(cre)Zman/J).

Procedures performed on the animals followed an experimental protocol approved by the University of Pittsburgh Institutional Animal Care and Use Committee (IACUC), also in accordance with the standards for humane animal care and use as set by the Animal Welfare Act and the National Institutes of Health Guide for the Care and Use of Laboratory Animals.

To place a cranial window, aseptic surgical procedures were followed for each animal. For surgery, animals were anesthetized using ketamine (75 mg/kg) and xylazine (10 mg/kg). The animals were then placed in a stereotaxic frame (Narishige, Tokyo, Japan) and supplementary

oxygen was administered at a rate of 500 mL/min using a nose cone (Narishige, Tokyo, Japan). Body temperature was maintained at 37°C during the duration surgery using a heating blanket with temperature feedback. Surgery consisted of incising the skin to expose the skull parietal bone over the somatosensory cortex. Acrylic cement was the applied to the surface of the parietal bone, surrounding an area slightly larger than 4x4 mm^2, and centered 2mm lateral and 1mm rostral from Bregma. A dental drill was used to remove the skull over the somatosensory cortex. In Thy1- and VGAT-ChR2-YFP animals, surgical light exposure to the brain during and after the craniotomy was filtered to green–yellow light (570±10 nm) to avoid exposure to white light, which could continuously stimulate the exposed brain tissue. In cre-recombinase animals, ChR2 expression was by viral injection in the somatosensory cortex. Virus encoding ChR2-YFP (AAV-EF1a-DIO-ChR2-YFP) was injected at depths of 300 μm and 600 μm into the somato-sensory cortex with a glass micropipette. Fluorescent dye (200 μM SR-101) was used to visualize virus delivery in the targeted locations, totaling an injection volume of about 0.1 μl. In all animals, a cover glass made in our lab consisting of a 4-mm round cover glass glued on a 5-mm round cover glass (CS-4R and CS-5R, Warner Instruments Inc.) was cemented onto the skull to seal the craniotomy while maintaining visual access of the brain. Animals were then returned to the cages and recover for 2-3 weeks following surgery. The mice were acclimated to a custom treadmill for awake head-fixed data collection staring approximately 1 week after surgery. In the NOS mouse model, Tamoxifen (75 mg/kg) was administered post-surgically 1-2 weeks, as described on the Jackson Laboratory's website, since it is an inducible creER line.

3.2 Data Acquisition

Two devices were simultaneously used to calculate $CMRO_2$ changes resulting from neuronal activity: (1) a laser Doppler flowmetry was used to measure CBF from the stimulated location within the imaging window, and (2) an optical imaging system was used to capture changes in the hemoglobin oxygenation state across the brain. Optical imaging was conducted by a camera with each frame sequentially illuminated by filtered light at 572 ± 7nm and 620 ± 7nm using light emitting diodes at an effective frame rate of 10 Hz per color. These wavelengths were chosen because of their extinction coefficients for HbR and HbO. At 572nm the absorption of HbO and HbR is about the same (isosbestic point) making it very sensitive to changes in CBV. At 620nm, the extinction coefficient of HbR is much greater (over 6x higher) than that of HbO making it very sensitive to change in blood oxygenation (BOLD). A laser doppler flow probe (Periflux 5000/411, Perimed AB, Jarfalla, Sweden) was used to assess cerebral blood flow (CBF) in sensory cortex, which sampled the blood flow at a rate of 100Hz. The LDF system operates at 785nm such that a short-pass filter (<700nm) was placed along the imaging path to block LDF illumination from the optical imaging system.

A power-adjustable, TTL-controlled, 473nm laser diode unit (CrystaLaser, Inc., Reno, NV) connected to the optic fiber with a core diameter of 200μm (FT-200-UMT, ThorLabs, Inc., Newton, NJ) was used to optogenetically activate ChR2 neurons. The laser was calibrated to deliver light of 1mW power at the output of the laser fiber using a power meter (Melles Griot 13PM001, IDEX Inc., Rochester, NY). A depiction of the imaging setup is shown in Figure 11.

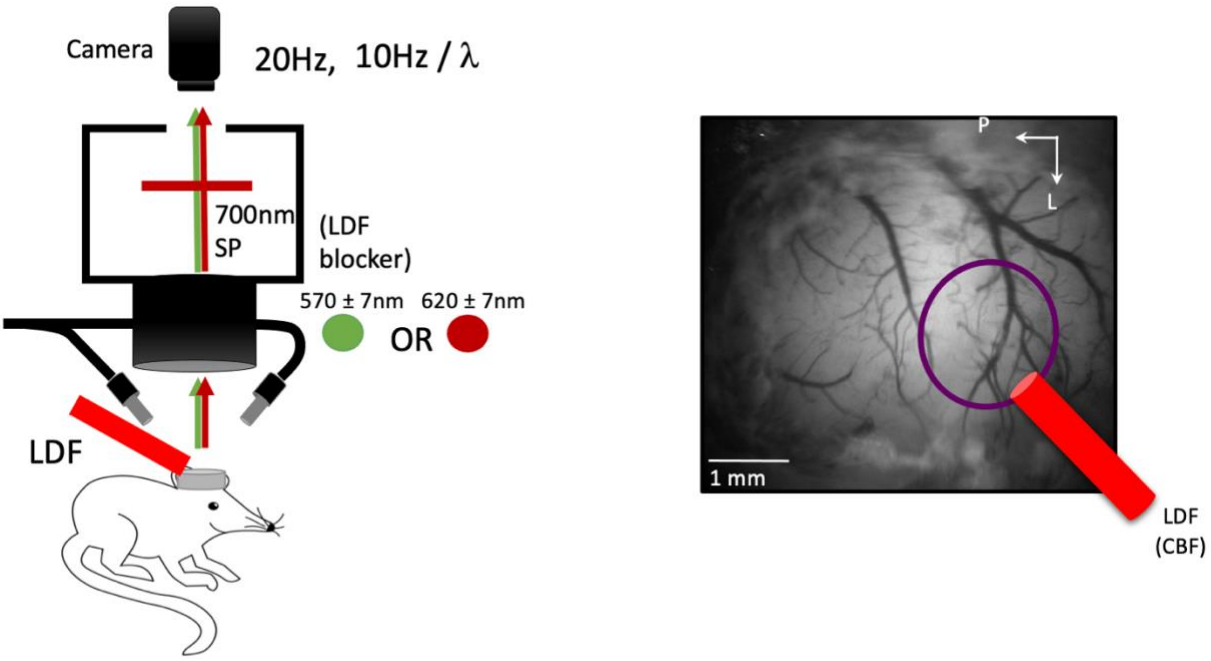

Figure 11. The imaging setup is depicted in the left panel. Images are acquired at 20Hz, or effectively 10Hz per wavelength. Two LEDs are used to illumine the brain at each wavelength. A laser doppler flow probe is also placed on the coverglass to record the cerebral blood flow. A 700nm shortpass optical filter is placed between the camera and the microscope to block the LDF artifact in the acquired image. A sample image also outlining the location of the LDF probe is shown in the right panel.

3.3 Experimental design

Experimentation was divided into three parts. In the first set of experiments, we set to verify that the $CMRO_2$ model (Eq. 13) can be used to make reasonable inferences of tissue oxygen metabolism. To this end, we conducted experiments while measuring LDF and OIS at 570 and 620nm during delivery of low-grade CO_2 (5-10%), and separately during delivery of air puffs to the mouse whisker pad to evoke neuronal activity in mouse somato-sensory cortex. We use the

CO_2 experiment data verify that the model in Eq. 13 calculates no general changes in $CMRO_2$ during CO_2 delivery ($rCMRO_2 = 1$). We also use this data to calibrate the model in Eq. 15. We then use the whisker stimulation data to compare $CMRO_2$ results from both models as well as their sensitivity. The second set of experiments, uses the model in Eq. 13 to calculate $CMRO_2$ from LDF and OIS at 570nm and 620nm data during optogenetic stimulation of the two major types of neurons. We compare these results to results previously obtained by our lab in anesthetized animals. Lastly, the third set of experiments uses the model in Eq. 13 to calculate $CMRO_2$ from LDF and OIS at 570nm and 620nm data during optogenetic stimulation of sub-types of inhibitory neurons.

3.3.1 $CMRO_2$ model test experiments

CO_2 calibration experiments were conducted using the same imaging and LDF probe setup described in section 3.2. The aim of the calibration experiments was to verify the 2-wavelength model produces no general changes in $CMRO_2$. We also use these data to compute β for the 1-wavelength model. Calibration was accomplished by subjecting the animal to a hypercapnic perturbation by sliding a nosecone over its snout to deliver a 7-10% CO_2 enhanced air mixture. Imaging occurred for 6.5 minutes, with a 30s pre-delivery period, 90s of CO_2 delivery, and 270s of post-CO_2-delivery imaging. The experimental setup with CO_2 delivery is depicted in Figure 12 (A).

The 1- wavelength and 2-wavelength models were then compared using whisker stimulation data. Whisker stimulation causes neuronal activation in the mouse barrel cortex, which can be recorded using the same imaging setup as described in section 3.2 with the addition of an air puffer to the deflect the whiskers on the whisker pad contralateral to the cranial window

location. The air puffs were delivered using a pressure injector (Toohey Spritzer, Toohey Company, Fairfield, NJ) with a pressure of 40-50 psi. Whisker puffs were delivered at a frequency of 5 Hz (50 ms puffs) for 4 seconds every 36 seconds repeated 12 times (Figure 12B).

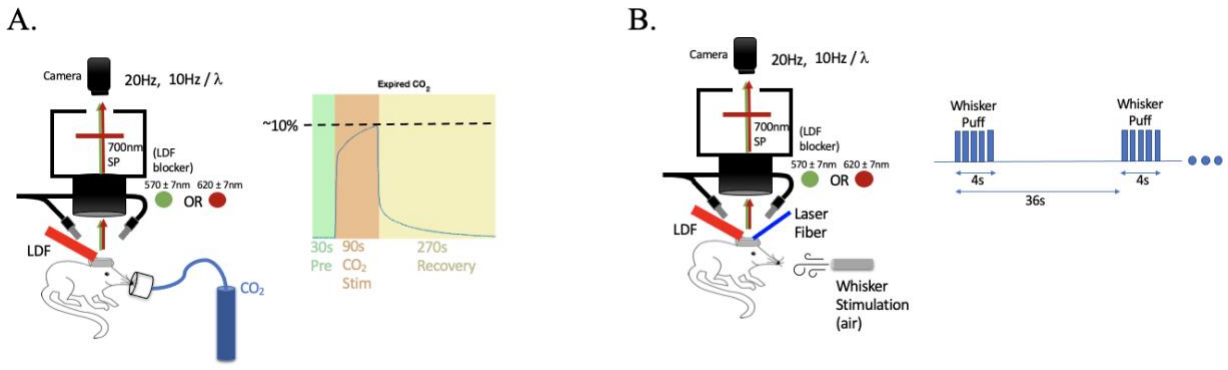

Figure 12. A) The imaging and experimental setup for the CO_2 calibration experiments. A trace of $\%CO_2$ on the outlet of the gas delivery system is shown. (B) The imaging and experimental setup for whisker stimulation to compare the 2 models of $rCMRO_2$ computation. The stimulation paradigm of the whisker puffing is also shown.

3.3.2 Optogenetic activation of Excitatory vs. Inhibitory neurons

Optogenetic activation experiments were conducted using the same imaging and LDF probe setup described in section 3.2. An optic fiber was placed on top of the cranial window facing the mouse somato-sensory cortex to deliver the optogenetic stimulus. Two optogenetic mouse models were used for these experiments targeting excitatory neurons (Thy1-ChR2) and inhibitory neurons (VGAT-ChR2). Optogenetic stimulation was conducted at several different frequencies and durations to manipulate the amount of activity generated by the targeted neuronal population.

The following stimulation parameters were tested: (1) 10ms pulses at 5 Hz for 1 second; (2) 10ms pulses at 40 Hz for 1 second; (3) 10ms pulses at 5 Hz for 4 seconds; (4) 30ms pulses at 5 Hz for 4 seconds; (5) 10ms pulses at 40 Hz for 4 seconds. Stimulation periods were repeated every 30 seconds and a total of 12 times. All optogenetic stimuli were delivered at 1mW laser power for inhibitory neurons (VGAT-ChR2), and at 0.25mW laser power for the excitatory neurons (Thy1-ChR2). The power of the laser was reduced in the Thy1-ChR2 neurons due to their abundance and extensive arborization in the brain, and the fact that over-stimulation of excitatory neurons can cause epileptogenic activity. Summary results were drawn from stimulation parameter (1), as this shortened pulse delivery elicited substantial changes in blood flow as well as measurable $CMRO_2$ changes while minimizing the overlap between the optogenetic light stimulus and our optical measurements. The experimental setup as well as stimulation paradigm of the optogenetic stimulation is depicted in Figure 13.

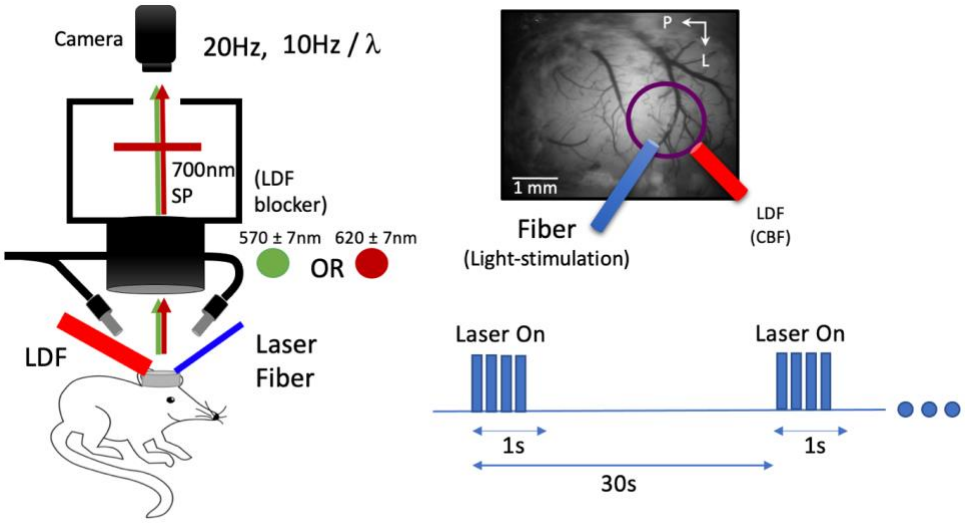

Figure 13. The imaging and experimental setup for the optogenetic experiments. The laser fiber placement is also shown on the image of the brain, and the stimulation parameters for the optogenetic stimulation are displayed on the bottom right of the figure.

Finally, to better investigate the changes of rCBF and $rCMRO_2$ caused by optogenetic stimulation in excitatory neurons alone, the pharmacological blockade agents APV and NBQX were applied in the cortex of Thy1 animal to block excitatory postsynaptic transmission. First, a baseline optogenetic stimulation experiment was done at the same stimulation parameters as previously described to characterize the neuronal function before pharmacological blockade. Then, the glass coverslip was removed, and the dural membrane exposed. A solution containing 5mM APV (Sigma-Aldrich, Inc.) and 1mM NBQX (Tocris Bioscience, Inc.) was topically applied to the surface of the dura. A large glass coverslip was applied on top of the well to minimize exposure of the brain to air, and 1 hour was allotted for the solution to permeate through the cortex. We verified through trials of stimulation of the forepaw in a separate experiment that excitatory neuronal transmission was not present for more than 2 hours after 1 hour of cortical exposure to the solution. After cortical exposure of 1 hour, we aspirated any solution still left in the craniotomy, and cemented the glass coverslip back to the skull. Optogenetic experimentation was then resumed as previously mentioned.

3.3.3 Optogenetic activation of Inhibitory neuron sub-types

The same experimental design described in 3.3.2 was used animals in this experimental group in the following models: PV-cre, VIP-cre, SOM-cre, NOS-cre, NPY-cre. The optic fiber was placed facing the virus injected region. We verified that the optogenetic expression of ChR2 spanned an area larger than the optogenetic stimulus. For these experiments, same optogenetic stimulus amplitude was used as that for VGAT-ChR2 animals (1mW).

3.4 Data analysis

All data was analyzed using MATLAB (MathWorks, MA, USA), and statistics were computed using Prism (GraphPad, CA, USA). The data from the LDF probe, which originally was sampled at 100Hz, was down sampled to 10Hz to match the imaging data in time. The imaging data were motion and intensity corrected. Motion correction consisted of a 2D Fourier-based translation-only rigid-body algorithm. The tenth image in each experimental run was used as reference. Intensity correction consisted of regressing the intensities observed in the corners of the images, on the skull, out of the image sequence. This was done because we expect no changes in signal coming from the skull, and thus considered such changes as unwanted artifacts. The 12 trials for each stimulation parameter, both for the imaging and LDF data were averaged to increase the signal to noise ratio. Masks were created over the cortex of the animal to map the regions of interest (ROIs) using the optogenetic light artifact as reference. We report magnitude changes as a result of the stimulation by averaging the samples which were above 80% of the peak blood flow and within 10s of the optogenetic stimulation. $CMRO_2$ was calculated using Eq. 13, setting γ_r and γ_t equal to 1, as is commonly done in the literature (4, 8).

The CO_2 perturbation data was only obtained over one trial, choosing the baseline and experimental conditions as an average of measurements before the CO_2 delivery and during the peak CO_2 delivery period. These data were then used to feed the models in Eq. 13 and 15 as well as to calculate the calibration coefficient β in Eq 16.

Finally, the optogenetic stimulus used provided blue-light illumination to a relatively fixed volume of tissue. The different models we used target a different number of cells over this volume of tissue. To account for the difference in the number of activated neurons upon optogenetic

stimulation for the different mouse models used, we compared the emission of YFP bound to ChR2 as an estimate of the number of cells activated by the optogenetic stimulus. Although we placed a filter in front of the camera to block the optogenetic stimulus, we remain sensitive to YFP emission because the optogenetic stimulus excites YFP with sufficient intensity to be detected at 570nm. For this calculation, the average image during the 40 Hz, 4s duration, 10ms pulse width stimulations was used. The 570nm channel was used, because YFP has larger emission contribution at 570nm than 620nm. Stimulation at 40Hz was used to ensure YFP-illuminated frames during the 10Hz imaging period. YFP quantification was accomplished by computing the percent change in camera signal during optogenetic stimulation relative to that before stimulation (dividing each pixel in the mean image during stimulation by the corresponding pixel in the mean image before stimulation). This allows for quantification of percent change in fluorescence over the brain as a result of the YFP emission. Since the same optogenetic stimulation parameters were used in all experiments, the illuminated area was approximately the same and the maximum YFP value (in %) in the stimulation region was used as an indicator of total YFP expression.

Statistics for changes in $CMRO_2$ were computed as two-sided, unpaired, parametric t-tests between the excitatory and inhibitory, as well as the excitatory with pharmacology and inhibitory groups. When comparing two groups, these tests were conducted as two-sample t-tests and significance established by corresponding p values less than 5%. These tests will be used to determine significant differences in blood flow as well as oxygen consumption. When comparing multiple groups for either changes in $CMRO_2$ or CBF, these tests will be conducted adjusting the p-value for the number of comparisons. Error bars and preliminary results of these t-tests will be reported in this work and are to illustrate the test criteria we will use to establish significance when the study is completed. To test model validity we will use a t-test to compare samples over the 30-

second period at the end of the hypercapnia period versus the 30-second period prior to hypercapnia onset for each animal as well as a population test across animals to test if $rCMRO_2$ is significantly different from 1.

4.0 Results

4.1 $CMRO_2$ model test experiments

Our first experimental group aimed to verify that the $CMRO_2$ model in Eq. 13 coupled with LDF and OIS data at two wavelengths (570nm and 620nm) can be used to calculate physiological changes in $CMRO_2$. To this end, LDF and OIS data at 570nm and 620nm were obtained from one animal during delivery of CO_2 for 90 seconds (Figure 14 shows the measurements in this animal). This manipulation intends to increase CBF while not changing $CMRO_2$. The changes in OIS signal was extracted over all tissue regions visible through the cranial window avoiding areas with visible surface vasculature. We found that CO_2 delivery of 7.2% produced an increase in rCBF of 91.29% ± 17.88% over the last 30-sec of hypercapnia and changes in $rCMRO_2$ of 0.17 ± 15.36%, and changes in OIS at 570nm and 620nm of -6.3% ± 1.7% and +1.7% ± 0.24%, respectively. The baseline period before CO_2 delivery showed a rCBF of 0.0 ± 8.0% and $rCMRO_2$ change of 1.5 ± 15.4%. Using these data on the model in Eq. 13 in one mouse shows that although LDF and OIS signals changes with CO_2 delivery, $rCMRO_2$ remains relatively close to 0% during the CO_2ß delivery period (Figure 14E). The spikes that are present in Figure 14E are likely the result of high ongoing neuronal activity periods since mice were awake during these experiments. Although the mean of the last 30 seconds during CO_2 delivery period shows an average $rCMRO_2$ of +12.6% for the 1-wavelength model, and -5.4% for the 2-wavelength model, the $rCMRO_2$ model successfully removed most of the CO_2-driven perturbation in the data supplied to it. A t-test yields that the rCBF change was significantly different from 0% during the hypercapnia period, with a $p < 0.0001$, and that the $rCMRO_2$ was not significantly different from 0% during that same time period, with

p=0.91. This reinforces our observation that the model was able to correctly compute no change in $CMRO_2$ despite a CBF increase. This gives us reasonable evidence that the 2-wavelength $CMRO_2$ model in Eq. 13 can be used to capture physiological changes in $CMRO_2$. We are currently planning to conduct additional experiments to make sure this effect is consistent in more than one animal.

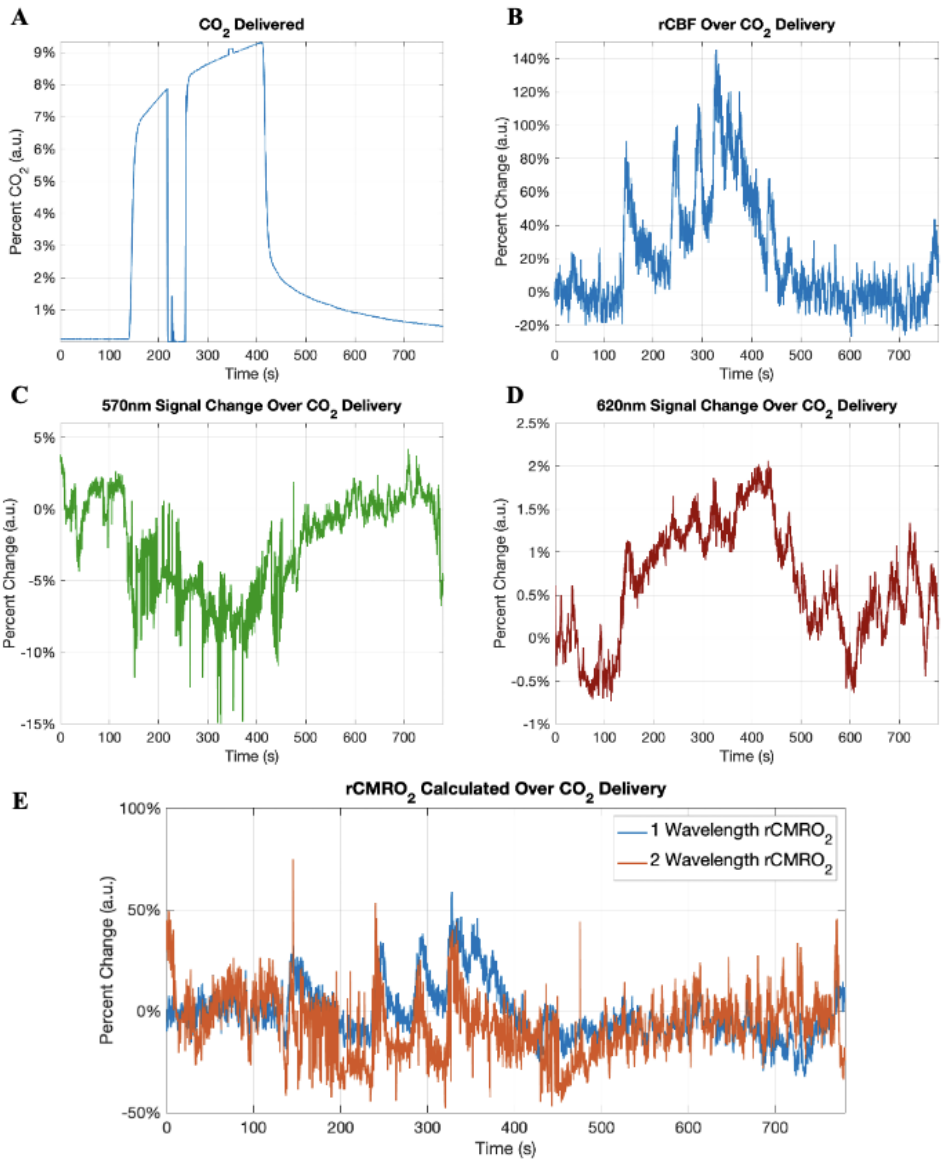

Figure 14. (A) %CO_2 administered over experiment duration. (B) rCBF change during CO_2 administration. (C-D) Optical imaging (570 and 620nm) signal changes in the LDF region. (E) $rCMRO_2$ computed from both the 1 wavelength and 2 wavelength model during CO_2 administration. The $rCMRO_2$ computed from both models hovers around 0%. The spikes in $rCMRO_2$ are most likely attributed to activity from the awake animal.

We then used the CO_2 data to calculate the calibration coefficient β and then use it to calculate $rCMRO_2$ using Eq. 15 (Figure 15, bottom panel). The value of β obtained for the animal

presented in Figure 14 was 15.4. We then use the calibration coefficient for that animal along with the whisker stimulation LDF and OIS data to compute $rCMRO_2$ during whisker evoked neuronal activity. The LDF probe was placed over somato-sensory cortex and OIS signals were extracted over tissue regions facing the LDF probe, excluding visible brain vasculature. Responses from one mouse are presented in Figure 15, where whisker stimulation produced increases in CBF of 70.3% and changes in OIS at 570nm and 620nm of -2.2% and +0.53%, respectively. In this animal, the $CMRO_2$ calculated from both models are shown in Figure 15. The mean $rCMRO_2$ as a result of whisker stimulation in the 1-wavelength model was 36.5%, and a change of 54.3% was computed using the 2-wavelength model. The last panel in Figure 15, below, shows the $rCMRO_2$ computed from each model, overlayed.

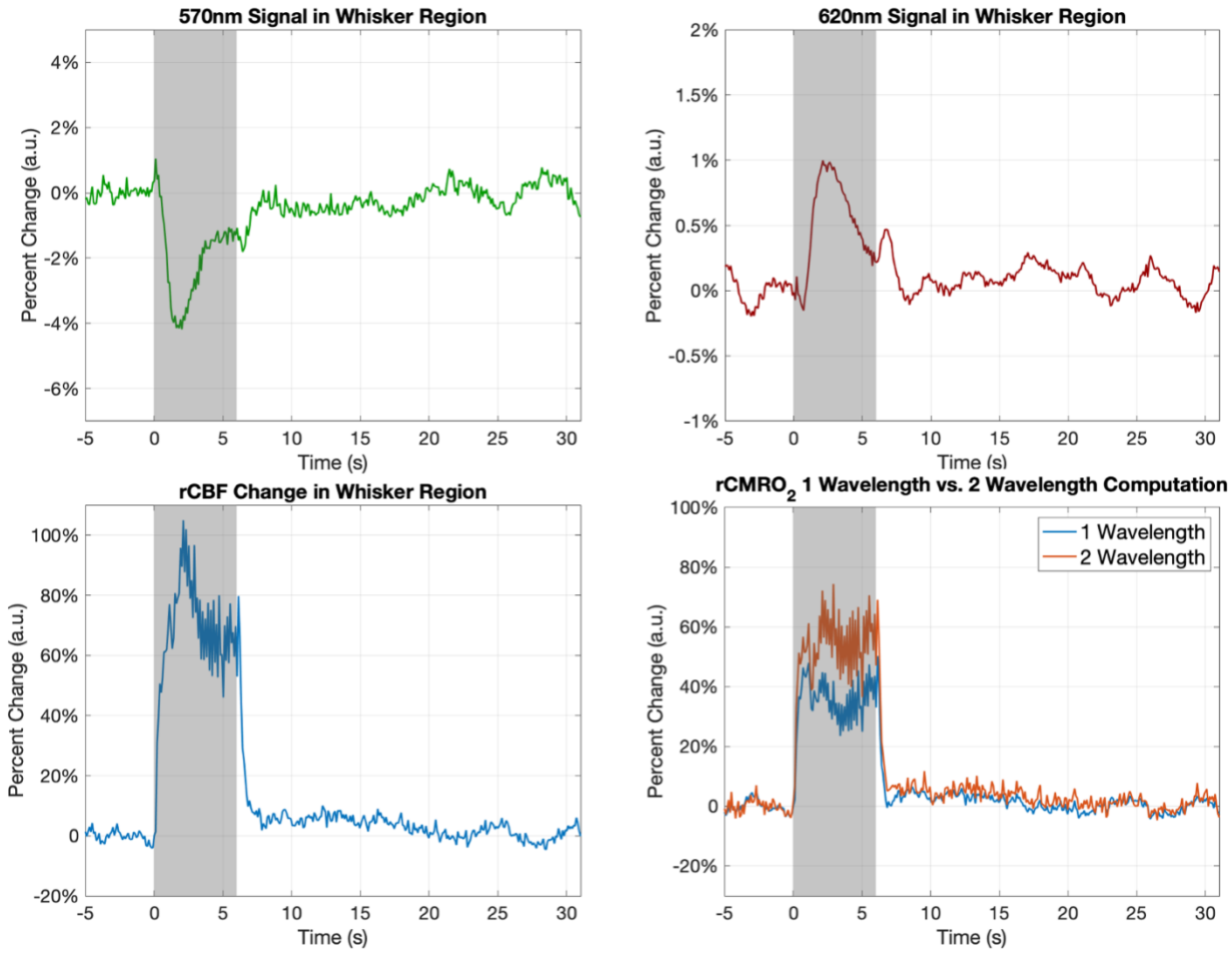

Figure 15. Changes in CBF measured by LDF and OIS signals at 570nm and 620nm during whisker stimulation. A region of interest was placed over the whisker somato-sensory cortex to obtain the average temporal signal changes at the imaged wavelengths. The last panel shows the computed $rCMRO_2$ change according to both the 1 wavelength and 2 wavelength models as a result of the whisker stimulation.

To increase the signal-to-noise ratio, we collect 16 trials of each whisker stimulation, and average them to represent the whisker response in that animal. Due to our low sample size for the calibration experiments, we chose to compute $rCMRO_2$ for each stimulation trial in this one animal and compare the performance of the calibrated 1-wavelength and the 2-wavelength models across these 16 trials. The average $rCMRO_2$ increase across 16 stimulations in the 1-wavelenght model was 36.2 ± 10.3% (SE), and 38 ± 11.2% in the 2-wavelength model. An unpaired t-test between

the 1-wavelength (n=16) and 2-wavelength (n=16) models showed no significance between their calculation of $rCMRO_2$, with a p value of p=0.81. This gives us reasonable support to continue using the 2-wavelength model to compute $rCMRO_2$ in our experiments, without the need to calibrate each experiment with CO_2.

4.2 Excitatory vs. Inhibitory CBF and $CRMO_2$

Optogenetic stimulation in Thy1-ChR2 and VGAT-ChR2 produced detectable CBF and OIS responses in all animals tested. Average OIS signals were extracted from the region faced by both the LDF probe and optic fiber. Significant CBF and OIS responses were obtained from optogenetic stimulation of both mouse models (Figure 16). Optogenetic stimulation introduced noticeable artifacts into the LDF traces, especially over onset and offset optogenetic stimulation periods. Because CBF and OIS responses appear to peak about 2-4 seconds after stimulation onset, we are only presenting responses to 1 second optogenetic stimulation responses. Average LDF, OIS 570 and OIS 620nm responses are presented in Table 1.

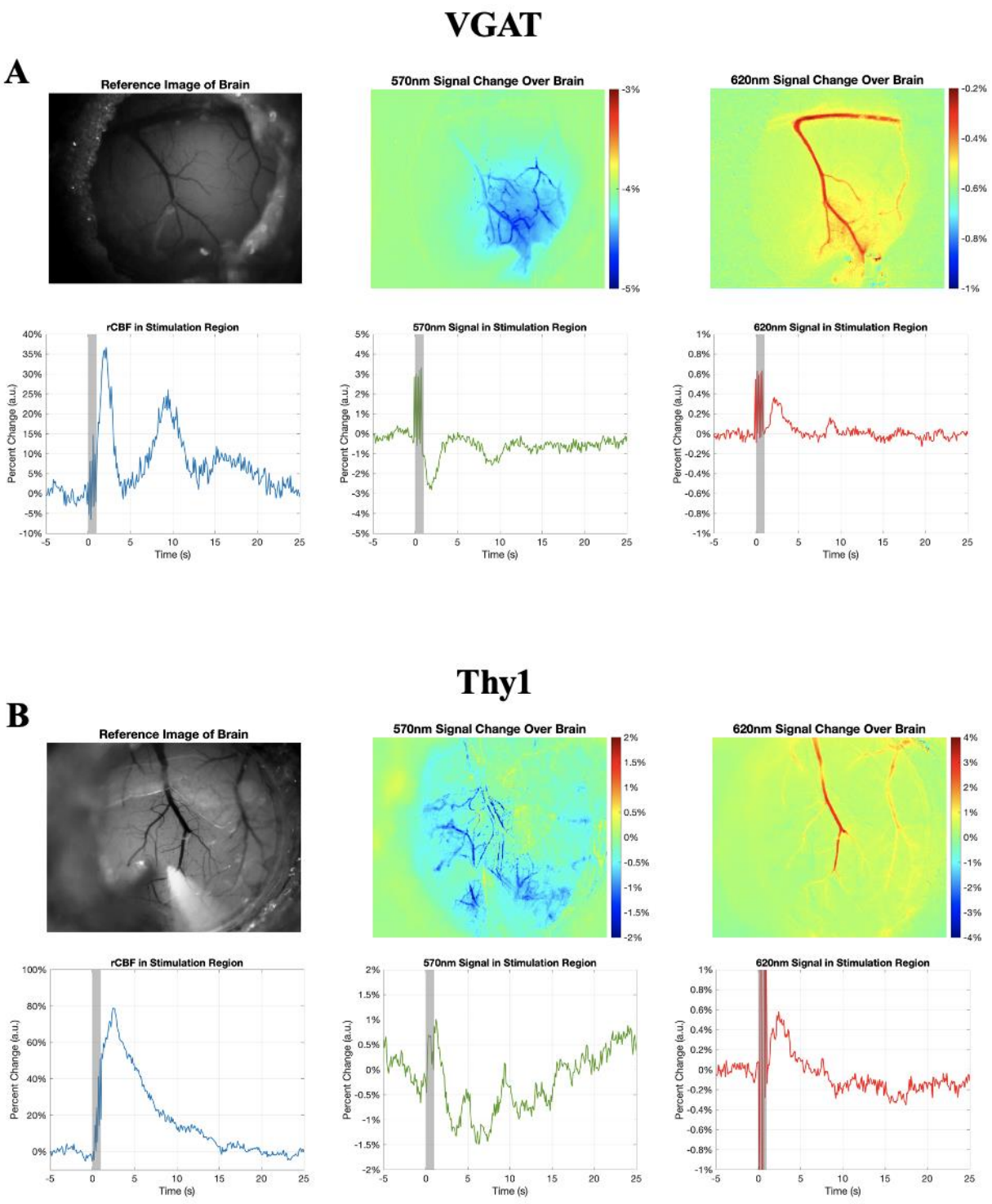

Figure 16. Changes in LDF, OIS 570 and 620 in a (A) VGAT, and (B) Thy1 animal. The changes across all acquisitions in both animals show significant increase from before the optogenetic stimulation.

Subsequently, $rCMRO_2$ was calculated using Eq. 13 from the LDF and OIS data. The average rCBF in the Thy1 animals was 50.4 ± 19.0 % and the mean $rCMRO_2$ calculated in the was 33.6 ± 16.3%. In VGAT animals, both the change in blood flow as well as the computed change in $CMRO_2$ were lower than Thy1. The average rCBF for VGAT animals was 22.2 ± 5.4% and the mean $rCMRO_2$ calculated was 10.5 ± 5.2%. On average, the CBF change in Thy1 animals was about 2.3 times larger than that measured in VGAT animals and the calculated $rCMRO_2$ was 3.2 times larger in Thy1 animals. These results alone seem to suggest that excitatory neurons consume more oxygen than inhibitory neurons. These results are shown in Figure 17 and summarized in Table 1.

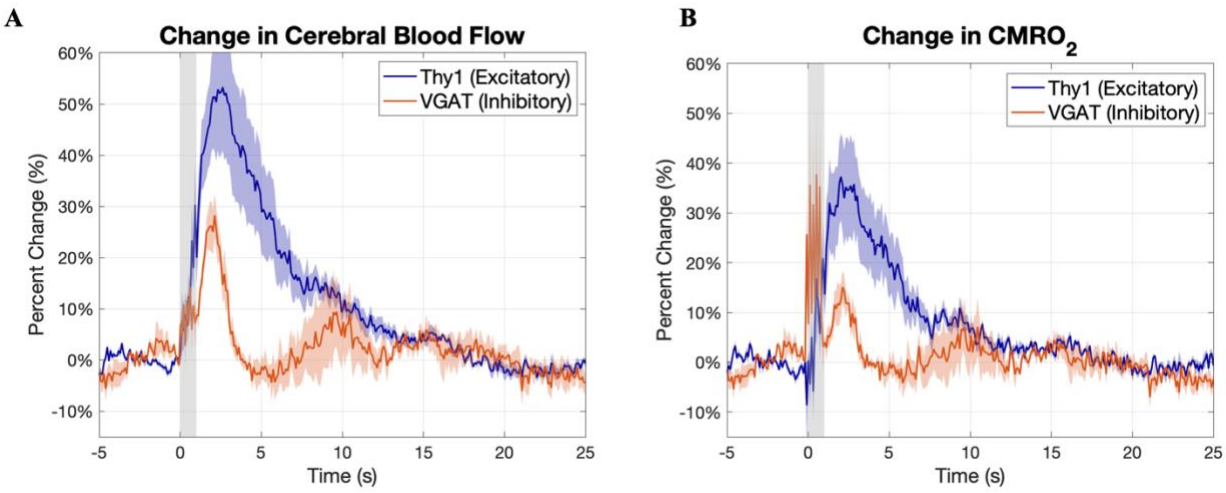

Figure 17. (A) The average measured rCBF across VGAT animals is shown as an orange trace, and the average rCBF across Thy1 animals is shown in blue. Shading denotes standard error of the mean. (B) The average computed $rCMRO_2$ across VGAT animals is shown in orange, and Thy1 in blue. Shading denotes standard error of the mean.

To examine the changes of rCBF and $rCMRO_2$ caused by optogenetic stimulation in excitatory neurons alone, a pharmacological strategy was used to block propagation of activity.

APV and NBQX were applied to the cortex of oneThy1 animal to block excitatory postsynaptic transmission. The resulting change in rCBF due to optogenetic stimulation after pharmacological blockade was 43.3%, and the change in $rCMRO_2$ was 13.9%. The measured change in CBF was not much different from the Thy1 animals without blockade but the computed $rCMRO_2$ was much lower. This suggests that a significant part of the calculated $CMRO_2$ response in the Thy1 animals without pharmacology may have been from post-synaptic neuronal activity. Considering these pharmacological results, the oxygen consumption ratio between excitatory and inhibitory neurons decreased from 3.2x to 1.3x (inhibitory/excitatory $rCMRO_2$ ratio of 0.76).

Since the number of neurons expressing ChR2 is different between models, we quantified the YFP emission produced by optogenetic stimulation as an indirect measure of the number of neurons expressing ChR2. We use the maximum YFP emission to compare against known differences in neuronal populations in mouse cortex. The mean maximum increase over the brain region for the Thy1 mice was 128.8%, and for the VGAT mice was 15.4%. The YFP emission in the Thy1 animals was, on average, 8.4x greater than that from the VGAT mice. This finding suggests that the change in $CMRO_2$ proportional to the number of neurons activated is far greater in VGAT animals than it is in Thy1 animals. After normalizing the calculated $rCMRO_2$ by the observed YFP increase by dividing the percent increase of $rCMRO_2$ by the increase in YFP emission during stimulation, the mean change in the Thy1 animals was 1.04, and the change in the VGAT animals was 7.20. Thus, this suggests that inhibitory neurons consume more oxygen by a factor of 6.9.

Table 1. Comparison of rCBF, $rCMRO_2$, rCBF/$rCMRO_2$ ratio, YFP emission, and $rCMRO_2$ normalized by YFP emission between Excitatory (Thy1) with and without pharmacology, and Inhibitory (VGAT).

	Excitatory (n=3)	Inhibitory (n=2)	Excitatory (Pharmacology) (n=1)
rCBF	50.35%	22.23%	43.30%
$rCMRO_2$	33.57%	10.46%	13.94%
rCBF/$rCMRO_2$	1.23	1.11	1.26
YFP	128.81%	15.35%	116.26%
$rCMRO_2$/YFP	1.037	7.20	0.98

4.3 Inhibitory Neuron sub-Population CBF and $CRMO_2$

Similar to Thy1 and VGAT neurons, optogenetic stimulation in all inhibitory neuronal subtypes produced detectable CBF and OIS responses in all animals tested. Inhibitory neurons tested include PV, VIP, SOM, NOS, and NPY. Similar to the results presented in the previous section, the optogenetic stimulation parameter for all mice is 10ms at 5Hz, since that stimulation parameter showed the best response across all neuronal subtypes. Figure 18 presents the LDF and OIS signal changes in an NPY animal.

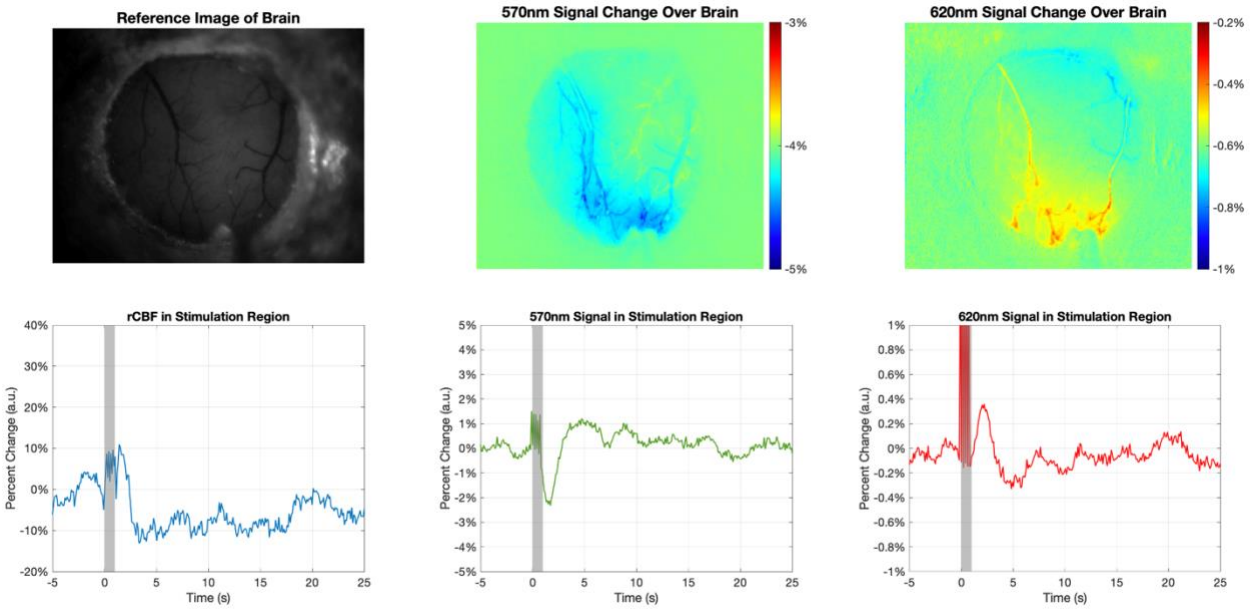

Figure 18. Changes in LDF, OIS 570 and 620 in a NPY animal. The changes across all acquisitions in both animals show significant increase from before the optogenetic stimulation.

Changes in CBF as well as $CMRO_2$ were also computed for the inhibitory subpopulations of neurons. The changes we noticed were for the most part similar to those in VGAT animals. In PV animals, the mean rCBF change was 2.1 ± 3.1%, and the mean $rCMRO_2$ was 1.2 ± 2.0%. Optogenetic stimulation of VIP neurons evoked a rCBF of 5.7%, and a $rCMRO_2$ of 3.4%. Upon stimulating SOM neurons, the mean rCBF was 18.8 ± 2.0%, and the mean $rCMRO_2$ was 7.9 ± 1.2%. In NOS animals, the mean rCBF was 8.9 ± 4.0%, and $rCMRO_2$ was 4.4 ± 2.1%. Finally, the rCBF was 12.4 ± 4.4% and the computed $rCMRO_2$ was 6.9 ± 5.8% for optogenetic stimulation of NPY neurons. The mean changes for rCBF as observed from the LDF probe and $rCMRO_2$ calculated in the optogenetic stimulation region across all neurons observed are summarized in Figure 19, as well as tabulated in Table 2. Interestingly, the average $CMRO_2$ change for VGAT animals was similar to the summation of the average PV, VIP and SOM $CMRO_2$ changes. Also,

SOM neurons provided the largest average CBF and $CMRO_2$ changes from any of the sub-types examined.

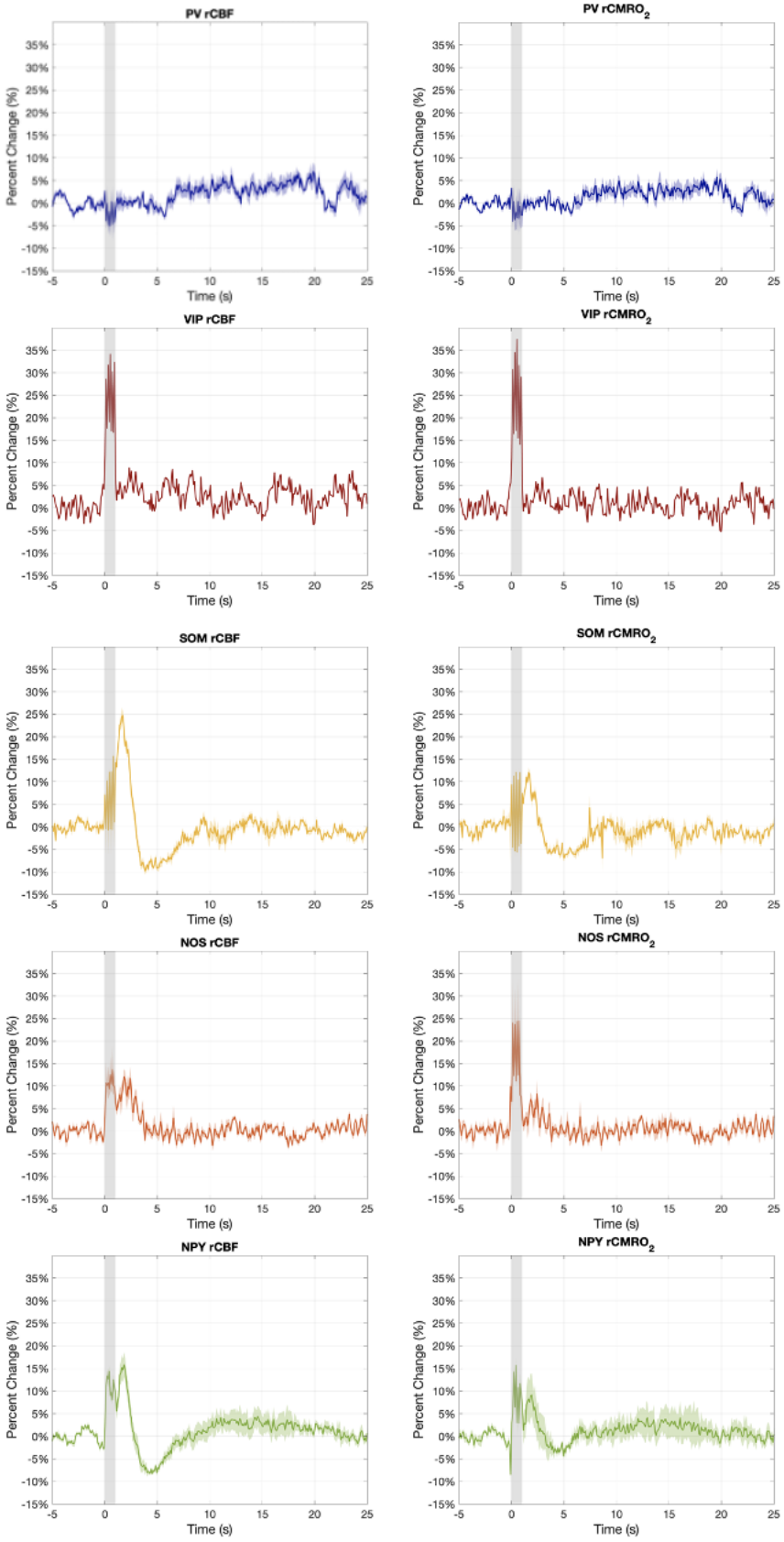
PV rCBF
PV rCMRO2
VIP rCBF
VIP rCMRO2
SOM rCBF
SOM rCMRO2
NOS rCBF
NOS rCMRO2
NPY rCBF
NPY rCMRO2
Percent Change (%)
Time (s)

Figure 19. rCBF and $rCMRO_2$ as a result of optogenetic stimulation across different inhibitory neuronal types. rCBF traces for each neuronal type are on the left, and $rCMRO_2$ traces are on the right.

Since the number of neurons expressing ChR2 differs between models, especially when ChR2 is inserted into the neurons via a viral vector, we quantified the YFP emission produced by optogenetic stimulation as an indirect measure of the number of neurons expressing the ChR2 protein. We use the maximum YFP emission to compare against known differences in neuronal populations in mouse cortex. The neuronal subpopulation YFP emissions were as follows: PV: 74.6%, VIP: 29.5%, SOM: 50.7%, NOS: 8.8%, and NPY: 89.9%.

Table 2. A summary of changes after optogenetic stimulation of subpopulations of inhibitory neurons. Each column denotes means for that neuronal type.

	VGAT (n=2)	**PV (n=3)**	**VIP (n=1)**	**SOM (n=3)**	**NOS (n=4)**	**NPY (n=4)**
rCBF	22.23%	2.09%	5.73%	18.75%	8.94%	12.37%
$rCMRO_2$	10.46%	1.21%	3.40%	7.94%	4.44%	6.85%
rCBF/$rCMRO_2$	1.11	1.01	1.02	1.10	1.04	1.05
YFP	15.35%	74.55%	29.52%	50.68%	8.81%	89.93%
$rCMRO_2$/YFP	7.20	1.36	3.50	2.13	11.85	1.19

5.0 Discussion

Experiments conducted using optogenetic stimulation of excitatory and inhibitory neurons show strong vascular and metabolic responses in the absence as well as presence of pharmacological agents to weight our results to the intended neuronal populations. When considering potential differences in the number of neurons activated, our results advocate for stronger contributions from inhibitory neurons to $CMRO_2$ than excitatory neurons. We attempted to verify that the model used can be sensitive to changes in tissue $CMRO_2$ using a physiological manipulation with known $CMRO_2$ and results from sensory activation. While these results provide some support for using the model, additional experiments are necessary to rigorously establish its use.

5.1 $CMRO_2$ model test experiments

We conducted other tests to verify whether the model which we use to calculate $rCMRO_2$ can be sensitive to tissue $CMRO_2$. For one of these tests, we used the imaging data with and without calibration to test each model. In this case, we used the rC_{HbT} data to estimate rCBF using the Grubb relationship. Then, we used the CO_2 data to compute the calibration coefficient β for every pixel within the imaged window (Figure 20). The calibration image shows that $\beta > 0$ for the most part. The value of β is close to zero over venous regions and is relatively high over arteries (>40). Figure 20 also show that β is relatively stable over tissue regions (~25).

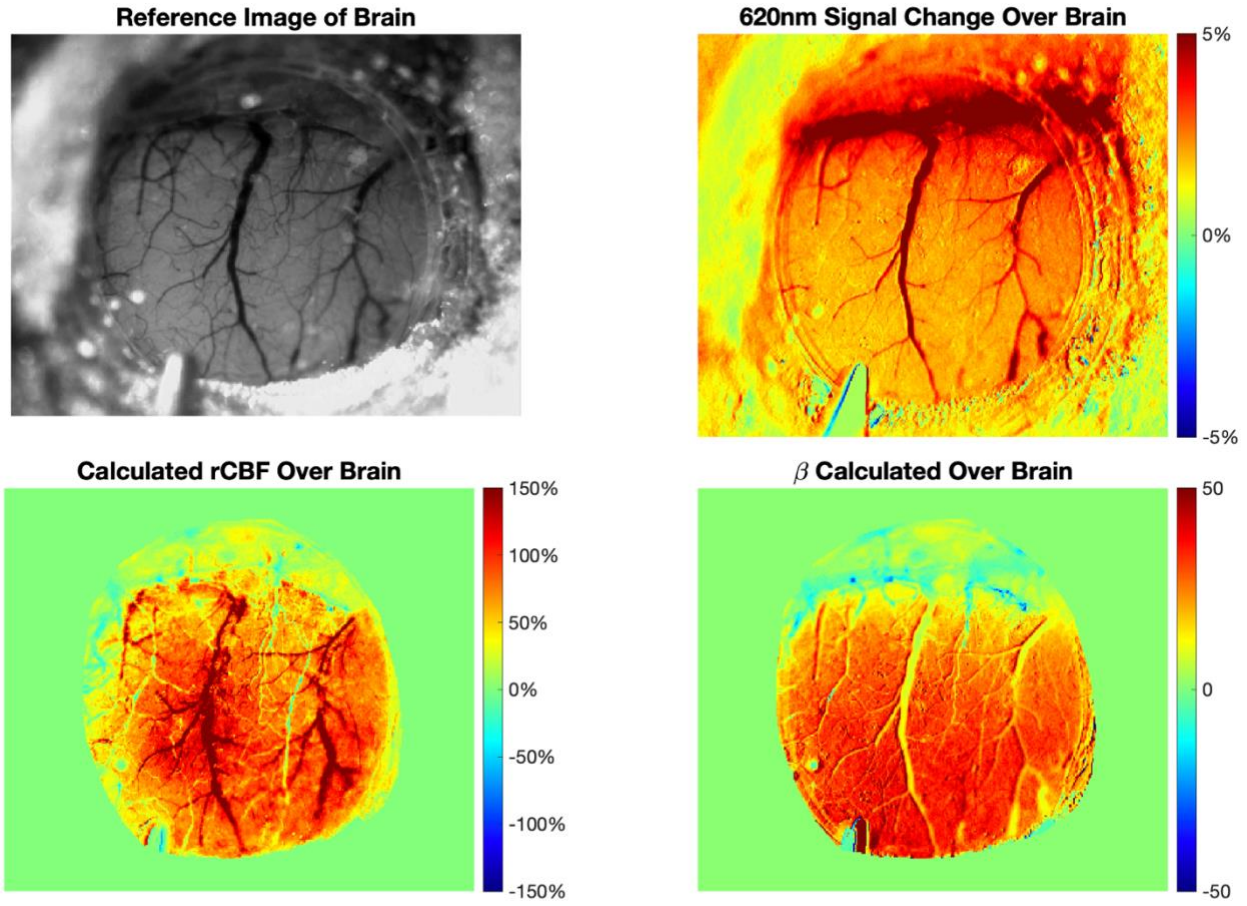

Figure 20. Pixelwise 620nm signal change, rCBF computed by Grubb's relation, and β computed pixelwise over the brain window.

We then used both models to calculate $CMRO_2$ across the brain window, using the pixelwise computed β in the 1-wavelength model's calculation. The computation of $rCMRO_2$ over the brain are shown in Figure 21. This provides some additional support for the 2-wavelength model. Through the pixelwise computation of $rCMRO_2$, we can see that the two models of $CMRO_2$ computation not only agree temporally, but spatially as well. Thus, we conclude that using the 2-wavelength model can be used to compute $rCMRO_2$, due to the simpler experimental setup, and the decreased spatial and temporal variability in the computed result.

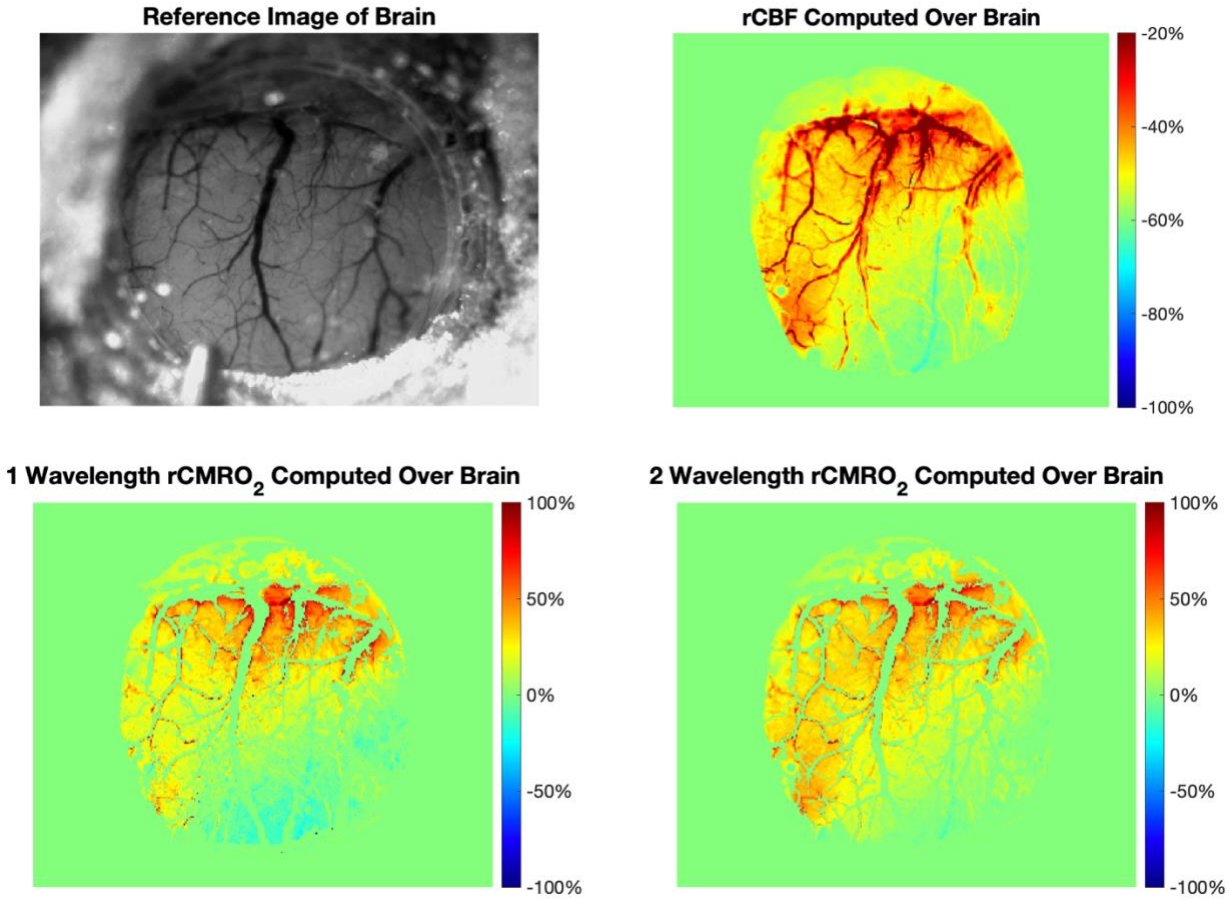

Figure 21. Pixelwise changes of rCBF and $rCMRO_2$ computed across the brain window. Blood vessels have been masked out using an intensity-based threshold of the reference image.

Testing the validation of the $CRMO_2$ model we use in these experiments can occur under any condition where both $rCMRO_2$ and rCBF changes are known. One of those conditions can be an increase in blood flow, but no change in oxygen consumption, as presented in previous results by administration of CO_2. Another modality in which we could test this model is a condition where blood flow remains constant, however oxygen consumption changes. This condition might be possible to achieve with anesthetics. Anesthetics are known to decrease neuronal activity, and thus oxygen consumption in the brain, but different anesthetics have varying effects on blood flow. Isoflurane is known to be a vasoactive anesthetic, however several studies have found that in low

amounts (<1.5%), blood flow is relatively unchanged in dogs (22, 23). The study by Stullken et al. also reported the $CMRO_2$ calculated as the difference in arterial and sagittal sinus O_2 concentration at each isoflurane concentration administered, and found that $CMRO_2$ decreased by ~25% with doses between 0.7% and 1.2% administered to the animals (22). We would then expect that administering a similar concentration to mice should keep CBF constant, and the computed $CMRO_2$ from our model should decrease by ~25% after administration of the drug. Other pharmacological agents could be used to achieve this conditions as well. For example, Nagaoka et. al. found that delivery of sodium nitroprusside did not change the cerebral blood flow in the cat cortex and increased the $CMRO_2$ (24). However, they did not report changes in $CMRO_2$. These conditions can be used to further evaluate the model described in this work.

5.2 Excitatory vs. Inhibitory CBF and $CRMO_2$

It is well known that excitatory neurons outnumber the inhibitory neurons in mouse cortex by about 4:1. Therefore, if excitatory and inhibitory neurons consume the same amount of oxygen upon stimulation, activation of the same volume of cortex by optogenetic stimulation would ideally show $rCMRO_2$ changes matching this proportion in Thy1:VGAT models. Since we do not know the exact number of cells expressing ChR2 in the models used, we relied on the YFP emission produced by optogenetic stimulation as an indirect measure. Our results show that $rCMRO_2$ in Thy1 mice is 3.2x larger than that of VGAT mice. However, when we scale $rCMRO_2$ by the YFP emission, the $rCMRO_2$ from VGAT mice exceed that of Thy1 mice by 6.92. This suggests that inhibitory neurons consume more oxygen than excitatory neurons.

In general, we would expect with our experimental protocol that the $CMRO_2$ response of excitatory neurons was over-estimated, and the $CMRO_2$ response of inhibitory neurons underestimated. This is because excitatory neurons excite post-synaptic excitatory and inhibitory neurons, potentially combining the response of many types of neurons. On the other hand, optogenetic stimulation of inhibitory neurons works to decrease the baseline activity of the brain. This effect adds decreases in activity over the metabolic response of inhibitory neurons. The way to control for these potential errors is to induce pharmacological blockade of neurons during the course of optogenetic stimulation experiments, which effectively blocks the excitatory effect of the excitatory neurons, and the inhibitory effect of the inhibitory neurons. We would expect that the magnitude of the excitatory neuronal activation is overestimated to a greater extent than the activation of inhibitory neurons is underestimated because our results show that inhibitory neurons have a significant change in $CMRO_2$ upon optogenetic stimulation. For these reasons, we decided to induce pharmacological blockade of excitatory neurons to gain a better understanding of the excitatory neuron $CMRO_2$ response. Our preliminary results suggest that a substantial part of the $rCMRO_2$ response of optogenetic stimulation of excitatory neurons without pharmacological blockade arises from the secondary transmission to inhibitory neurons.

Although additional experimentation is necessary to isolate neuronal activity to ChR2-positive neurons alone, experiments under anesthesia have shed some light on this potential issue. In a study previously performed by our laboratory in anesthetized mice, we found $rCMRO_2$ changes of +1.5% in Thy1 mice and -5% in VGAT mice, showing the effect of inhibition on overall brain metabolism. After pharmacological blockade of neurotransmission (only done in VGAT mice), optogenetic stimulation evoked an increase in $rCMRO_2$ of +3.9% (4). Since the effect of inhibition was noticed in the inhibitory no blockade group, we cannot infer the true oxygen

consumption from the $rCMRO_2$ computed, and thus must compare the excitatory $rCMRO_2$ (+1.5%) to the inhibitory with blockade group (+3.9%). This study then implies that inhibitory neurons consume 2.6x more oxygen than excitatory neurons. In general, these findings were similar to those obtained in two other studies using similar but not identical conditions and mouse models (2-4). Below, Table 3 summarizes the results of Vazquez et al., the study with almost identical experimental conditions performed in our laboratory in anesthetized mice.

Table 3. Results from a study conducted in our laboratory in 2018 with anesthetized Thy1 and VGAT animals (4). "Excitatory" denotes Thy1-ChR2 animals, while "Inhibitory" denotes VGAT-ChR2 animals.

	Anesthetized Excitatory	**Anesthetized Inhibitory - No Blockade**	**Anesthetized Inhibitory - Blockade**
rCBF	3.40%	16.00%	17.20%
$rCMRO_2$	1.50%	-1.50%	3.90%
rCBF/$rCMRO_2$	3.40	-10.67	4.41

Comparing these results with the ones from our experimentation, we notice several differences. The first is that both rCBF and oxygen metabolism are markedly decreased in the anesthetized condition. Additionally, in the anesthetized condition, we notice a higher rCBF:$rCMRO_2$ ratio. This suggest that the awake brain extracts more O_2 for the same blood flow than the anesthetized brain. We also notice the effects of inhibition upon stimulation of inhibitory neurons in anesthetized animals, having increased rCBF but decreased $rCMRO_2$. This effect, however, is reversed upon administration of pharmacological agents which block Glutamate and $GABA_A$ receptors. The inhibition effect upon stimulating inhibitory neurons in awake animals is not noticed, most likely due to greater neural activity upon stimulation of an awake animal. Despite

some differences in results, both awake and anesthetized results support the notion that inhibitory neurons consume more oxygen than excitatory neurons, despite their numbers and differences in anatomy and arborization extent.

It is important to note that the $rCMRO_2$ response computed depend on γ_r and γ_t values, as well as the initial concentration of HbR and HbT, as shown in Eq. 6. We assumed γ_r and γ_t values to be 1 in this study, which we know to not always be true areas with fewer capillaries, where signal contribution from arteries and veins is not equal. Additionally, initial concentrations of HbR and HbT were assumed to be 40μM and 100μM, respectively. These values are commonly assumed in the literature (4, 8), however can impact the computed $rCMRO_2$. Future studies will be aimed at consolidating these assumptions.

Despite assumptions made in the model, our finding that inhibitory neurons are more metabolically expensive to operate have been suggested in studies using other modalities of investigation. In 2015, Kasthuri's group aimed to determine the structure and composition of neural tissue using scanning electron microscopy. While determining differences in the structure of excitatory and inhibitory neurons, they noticed that mitochondria occupy twice as much volume in the inhibitory dendrites than they do in the excitatory dendrites (25). This supports our findings because larger mitochondrial volume is indicative of larger metabolic needs, and therefore higher oxygen consumption. Another group found, using immunohistochemical staining to identify excitatory and inhibitory neurons combined with imaging sensitive to glucose consumption, that inhibitory neurons were much more metabolically active than excitatory neurons upon whisker stimulation (26). Glucose consumption is another marker for metabolic activity and is linked with oxygen consumption as they are both metabolites in the Citric Acid Cycle. Thus, the increased glucose consumption in this study is consistent with the results we presented in our study.

5.3 Inhibitory Neuron sub-Population Discussion

The results of the inhibitory neuron sub-population optogenetic stimulation trials show differences in the magnitude and shape of rCBF as well as $rCMRO_2$ response. From Figure 19, we notice two similar general trends: one trend is that following optogenetic stimulation, there is a sharp and short increase in rCBF and $rCMRO_2$, and following that increase, we notice a significant decrease. The neurons which follow this trend are SOM, NOS, and NPY. In another group, there seems to be no real increase in blood flow, and only a slight, if at all, increase in $rCMRO_2$ (Figure 19). The neurons in this category are PV and VIP. This delineation of groups, suggested by the data, is corroborated by the composition of SOM neuronal group since SOM neurons are made up by multiple subtypes of inhibitory neurons, two of which include NOS and NPY.

Additionally, the temporal shapes of the rCBF and $rCMRO_2$ in VGAT resembles that of the shapes of the inhibitory subtypes, mainly driven by the SOM neuronal group. This is good verification that the VGAT animals are truly a representation of the inhibitory neuronal subtypes as a whole. While more animals need to be added to our sample size to investigate quantitative and statistical differences in blood flow and oxygen metabolism response between the subtypes, these preliminary results suggest that these differences in response do exist.

Finally, we comment on the blood flow regulation as well as oxygen consumption of the inhibitory neuronal subpopulations. Our results suggest that the SOM, NOS, and NPY animals are the strongest regulators of CBF, while PV and VIP animals are poor regulators of CBF. The results also suggest that $rCMRO_2$ is correlated with the rCBF response in the inhibitory subtypes, as the neurons with higher rCBF also had higher $rCMRO_2$ changes. Future studies, though, will be aimed at increasing the sample size of some of the inhibitory populations as well observing the effects of stimulating at higher frequencies and longer pulse widths.

6.0 Future directions

This project is the first to directly compare $rCMRO_2$ between inhibitory and excitatory neurons in the same experimental conditions in awake mice. In this coming year, we plan to expand this study and increase the sample size of Thy1 and VGAT mice to n=6, and Thy1 mice with pharmacology to n=4. Increasing the sample size will increase the power behind our findings comparing excitatory and inhibitory neuron oxygen consumption. Additionally, we will increase the sample size of PV mice to n=6 and VIP mice to n=4, to capture a more representative CBF and $CMRO_2$ regulation of these inhibitory neuronal subtypes. We will also analyze and incorporate data we have acquired for optogenetic stimulation at higher frequencies (20 and 40 Hz with 10ms pulse width). This will help determine whether $CMRO_2$ is activity-dependent since higher frequency stimulation should elicit more activity. I will also attempt to incorporate 4 second data by reducing the artifacts in the time series to better observe the changes of interest.

In the future, $rCMRO_2$ computation along with optogenetic modulation of neuronal subtypes can be used to understand the interactions and dysregulation between neurons in different disease of the brain. It is known that certain diseases such as epilepsy, Alzheimer's Disease, and schizophrenia have a component of excitatory-inhibitory neuronal dysfunction. Thus, comparing the rCBF, $rCMRO_2$, and electrophysiological responses of different subtypes of neurons in animal groups with and without these diseased neurons may point to specific neuronal subtypes which can be responsible for dysfunction across neuronal networks of the brain.

Bibliography

1. Keller D, Ero C, Markram H. Cell Densities in the Mouse Brain: A Systematic Review. Front Neuroanat. 2018;12:83. Epub 20181023. doi: 10.3389/fnana.2018.00083. PubMed PMID: 30405363; PubMed Central PMCID: PMC6205984.

2. Dahlqvist MK, Thomsen KJ, Postnov DD, Lauritzen MJ. Modification of oxygen consumption and blood flow in mouse somatosensory cortex by cell-type-specific neuronal activity. J Cereb Blood Flow Metab. 2020;40(10):2010-25. Epub 20191023. doi: 10.1177/0271678X19882787. PubMed PMID: 31645177; PubMed Central PMCID: PMC7786843.

3. Lee J, Stile CL, Bice AR, Rosenthal ZP, Yan P, Snyder AZ, et al. Opposed hemodynamic responses following increased excitation and parvalbumin-based inhibition. J Cereb Blood Flow Metab. 2021;41(4):841-56. Epub 20200617. doi: 10.1177/0271678X20930831. PubMed PMID: 33736512; PubMed Central PMCID: PMC7983494.

4. Vazquez AL, Fukuda M, Kim SG. Inhibitory Neuron Activity Contributions to Hemodynamic Responses and Metabolic Load Examined Using an Inhibitory Optogenetic Mouse Model. Cereb Cortex. 2018;28(11):4105-19. doi: 10.1093/cercor/bhy225. PubMed PMID: 30215693; PubMed Central PMCID: PMC6188559.

5. Mintun MA, Raichle ME, Martin WR, Herscovitch P. Brain oxygen utilization measured with O-15 radiotracers and positron emission tomography. J Nucl Med. 1984;25(2):177-87. PubMed PMID: 6610032.

6. Piilgaard H, Lauritzen M. Persistent increase in oxygen consumption and impaired neurovascular coupling after spreading depression in rat neocortex. J Cereb Blood Flow Metab. 2009;29(9):1517-27. Epub 20090610. doi: 10.1038/jcbfm.2009.73. PubMed PMID: 19513087.

7. Ma Y, Shaik MA, Kim SH, Kozberg MG, Thibodeaux DN, Zhao HT, et al. Wide-field optical mapping of neural activity and brain haemodynamics: considerations and novel approaches. Philos Trans R Soc Lond B Biol Sci. 2016;371(1705). doi: 10.1098/rstb.2015.0360. PubMed PMID: 27574312; PubMed Central PMCID: PMC5003860.

8. Dunn AK, Devor A, Dale AM, Boas DA. Spatial extent of oxygen metabolism and hemodynamic changes during functional activation of the rat somatosensory cortex. Neuroimage. 2005;27(2):279-90. doi: 10.1016/j.neuroimage.2005.04.024. PubMed PMID: 15925522.

9. Nagy A. Cre recombinase: the universal reagent for genome tailoring. Genesis. 2000;26(2):99-109. PubMed PMID: 10686599.

10. Wang H, Peca J, Matsuzaki M, Matsuzaki K, Noguchi J, Qiu L, et al. High-speed mapping of synaptic connectivity using photostimulation in Channelrhodopsin-2 transgenic mice. Proc Natl

Acad Sci U S A. 2007;104(19):8143-8. Epub 20070501. doi: 10.1073/pnas.0700384104. PubMed PMID: 17483470; PubMed Central PMCID: PMC1876585.

11. Arenkiel BR, Peca J, Davison IG, Feliciano C, Deisseroth K, Augustine GJ, et al. In vivo light-induced activation of neural circuitry in transgenic mice expressing channelrhodopsin-2. Neuron. 2007;54(2):205-18. doi: 10.1016/j.neuron.2007.03.005. PubMed PMID: 17442243; PubMed Central PMCID: PMC3634585.

12. Krawchuk MB, Ruff CF, Yang X, Ross SE, Vazquez AL. Optogenetic assessment of VIP, PV, SOM and NOS inhibitory neuron activity and cerebral blood flow regulation in mouse somato-sensory cortex. J Cereb Blood Flow Metab. 2020;40(7):1427-40. Epub 20190816. doi: 10.1177/0271678X19870105. PubMed PMID: 31418628; PubMed Central PMCID: PMC7307010.

13. Kitaura H, Uozumi N, Tohmi M, Yamazaki M, Sakimura K, Kudoh M, et al. Roles of nitric oxide as a vasodilator in neurovascular coupling of mouse somatosensory cortex. Neurosci Res. 2007;59(2):160-71. Epub 20070622. doi: 10.1016/j.neures.2007.06.1469. PubMed PMID: 17655958.

14. Yavorska I, Wehr M. Somatostatin-Expressing Inhibitory Interneurons in Cortical Circuits. Front Neural Circuits. 2016;10:76. Epub 20160929. doi: 10.3389/fncir.2016.00076. PubMed PMID: 27746722; PubMed Central PMCID: PMC5040712.

15. Zhao S, Ting JT, Atallah HE, Qiu L, Tan J, Gloss B, et al. Cell type-specific channelrhodopsin-2 transgenic mice for optogenetic dissection of neural circuitry function. Nat Methods. 2011;8(9):745-52. doi: 10.1038/nmeth.1668. PubMed PMID: 21985008; PubMed Central PMCID: PMC3191888.

16. Gonchar Y, Wang Q, Burkhalter A. Multiple distinct subtypes of GABAergic neurons in mouse visual cortex identified by triple immunostaining. Front Neuroanat. 2007;1:3. Epub 20080328. doi: 10.3389/neuro.05.003.2007. PubMed PMID: 18958197; PubMed Central PMCID: PMC2525923.

17. Tricoire L, Vitalis T. Neuronal nitric oxide synthase expressing neurons: a journey from birth to neuronal circuits. Front Neural Circuits. 2012;6:82. Epub 20121205. doi: 10.3389/fncir.2012.00082. PubMed PMID: 23227003; PubMed Central PMCID: PMC3514612.

18. Morton GJ, Schwartz MW. The NPY/AgRP neuron and energy homeostasis. Int J Obes Relat Metab Disord. 2001;25 Suppl 5:S56-62. doi: 10.1038/sj.ijo.0801915. PubMed PMID: 11840217.

19. Grubb RL, Jr., Raichle ME, Eichling JO, Ter-Pogossian MM. The effects of changes in PaCO2 on cerebral blood volume, blood flow, and vascular mean transit time. Stroke. 1974;5(5):630-9. doi: 10.1161/01.str.5.5.630. PubMed PMID: 4472361.

20. Davis TL, Kwong KK, Weisskoff RM, Rosen BR. Calibrated functional MRI: mapping the dynamics of oxidative metabolism. Proc Natl Acad Sci U S A. 1998;95(4):1834-9. doi: 10.1073/pnas.95.4.1834. PubMed PMID: 9465103; PubMed Central PMCID: PMC19199.

21. Hoge RD, Atkinson J, Gill B, Crelier GR, Marrett S, Pike GB. Investigation of BOLD signal dependence on cerebral blood flow and oxygen consumption: the deoxyhemoglobin dilution model. Magn Reson Med. 1999;42(5):849-63. doi: 10.1002/(sici)1522-2594(199911)42:5<849::aid-mrm4>3.0.co;2-z. PubMed PMID: 10542343.

22. Stullken EH, Jr., Milde JH, Michenfelder JD, Tinker JH. The nonlinear responses of cerebral metabolism to low concentrations of halothane, enflurane, isoflurane, and thiopental. Anesthesiology. 1977;46(1):28-34. doi: 10.1097/00000542-197701000-00007. PubMed PMID: 831591.

23. Roald OK, Forsman M, Steen PA. The effects of prolonged isoflurane anaesthesia on cerebral blood flow and metabolism in the dog. Acta Anaesthesiol Scand. 1989;33(3):210-3. doi: 10.1111/j.1399-6576.1989.tb02892.x. PubMed PMID: 2728824.

24. Nagaoka T, Zhao F, Wang P, Harel N, Kennan RP, Ogawa S, et al. Increases in oxygen consumption without cerebral blood volume change during visual stimulation under hypotension condition. J Cereb Blood Flow Metab. 2006;26(8):1043-51. Epub 20051214. doi: 10.1038/sj.jcbfm.9600251. PubMed PMID: 16395284.

25. Kasthuri N, Hayworth KJ, Berger DR, Schalek RL, Conchello JA, Knowles-Barley S, et al. Saturated Reconstruction of a Volume of Neocortex. Cell. 2015;162(3):648-61. doi: 10.1016/j.cell.2015.06.054. PubMed PMID: 26232230.

26. McCasland JS, Hibbard LS. GABAergic neurons in barrel cortex show strong, whisker-dependent metabolic activation during normal behavior. J Neurosci. 1997;17(14):5509-27. PubMed PMID: 9204933; PubMed Central PMCID: PMC6793834.